iScience

CellPress

Article

Loss of RNA-Binding Protein *Sfpq* Causes Long-Gene Transcriptopathy in Skeletal Muscle and Severe Muscle Mass Reduction with Metabolic Myopathy

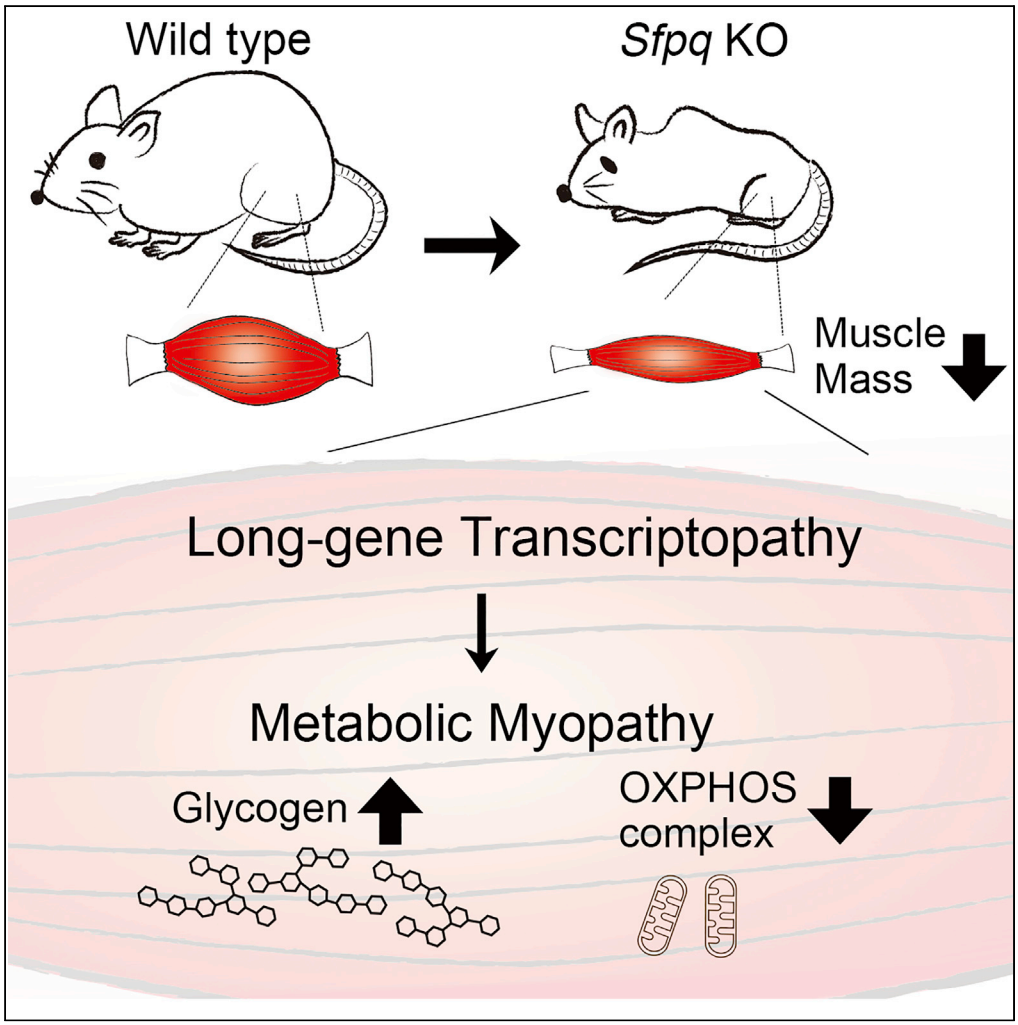

Motoyasu Hosokawa, Akihide Takeuchi, Jun Tanihata, Kei Iida, Shin'ichi Takeda, Masatoshi Hagiwara

takeuchi.akihide.8r@kyoto-u.ac.jp (A.T.)
hagiwara.masatoshi.8c@kyoto-u.ac.jp (M.H.)

HIGHLIGHTS

SFPQ is essential for long gene expression, including *Dystrophin*, in skeletal muscle

Disruption of *Sfpq* caused severe muscle mass reduction and premature death

SFPQ is required for metabolic pathway gene expression in skeletal muscle

Loss of *Sfpq* decreased OXPHOS complexes and caused glycogen accumulation

Hosokawa et al., iScience *13*, 229–242
March 29, 2019
https://doi.org/10.1016/j.isci.2019.02.023

iScience

CellPress

Article

Loss of RNA-Binding Protein *Sfpq* Causes Long-Gene Transcriptopathy in Skeletal Muscle and Severe Muscle Mass Reduction with Metabolic Myopathy

Motoyasu Hosokawa,[1,2] Akihide Takeuchi,[1,5,*] Jun Tanihata,[2,3] Kei Iida,[4] Shin'ichi Takeda,[2] and Masatoshi Hagiwara[1,*]

SUMMARY

Growing evidences are suggesting that extra-long genes in mammals are vulnerable for full-gene length transcription and dysregulation of long genes is a mechanism underlying human genetic disorders. How long-distance transcription is achieved is a fundamental question to be elucidated. In previous study, we had discovered that RNA-binding protein SFPQ preferentially binds to long pre-mRNAs and specifically regulates the cluster of neuronal genes >100 kbp. Here we investigated the roles of SFPQ for long gene expression, target specificities, and also physiological functions in skeletal muscle. Loss of *Sfpq* selectively downregulated genes >100 kbp including *Dystrophin*, which is 2.26 Mbp in length. *Sfpq* knockout (KO) mice showed progressive muscle mass reduction and metabolic myopathy characterized by glycogen accumulation and decreased abundance of mitochondrial oxidative phosphorylation complexes. Functional clustering analysis identified energy metabolism pathway genes as SFPQ's targets. These findings indicate target gene specificities and tissue-specific physiological functions of SFPQ in skeletal muscle.

INTRODUCTION

Evolutionarily, genome size and gene length of vertebrates are quite expanded and pre-mRNA transcripts expressed in mammals, especially in brains, are significantly longer (Gabel et al., 2015; Polymenidou et al., 2011). It has been suggested that extra-long genes are subjects of specific regulatory machineries that sustain their long-distance transcription. For long gene transcription, RNA-binding proteins (RBPs) or splicing factors have been demonstrated to play central roles as shown in SFPQ, FUS, TDP-43 (Lagier-Tourenne et al., 2012; Polymenidou et al., 2011; Takeuchi et al., 2018), or U1 snRNP (Oh et al., 2017). In addition, dysregulations of long gene transcription have been revealed as the causes of several genetic diseases in human, such as neurodegenerative and psychiatric diseases (Cortese et al., 2014; Gabel et al., 2015; King et al., 2013; Lagier-Tourenne et al., 2012; Polymenidou et al., 2011; Rogelj et al., 2012; Sugino et al., 2014).

In our previous study, we found that SFPQ is a key regulator of long genes in brain that sustains the full-gene length transcription through serially activating RNA polymerase II during transcriptional elongation. SFPQ preferentially binds to genes harboring GA- and CA-repeats in their long introns. Neuron-specific disruption of *Sfpq* resulted in the downregulation of long genes essential for brain formation and caused neural apoptosis. We have termed this selected disruption of long-gene expression as "long-gene transcriptopathy" (Takeuchi et al., 2018). Skeletal muscle is known to express several extra-long genes longer than 100 kbp, such as *Dystrophin* (*Dmd*, 2.26 Mbp), *Titin* (*Ttn*, 279 kbp), *Dysferlin* (*Dysf*, 202 kbp), and *Sarcoglycan delta* (*Sgcd*, 1.09 Mbp), which are essential for structures or motor functions of skeletal muscle cells, and mutations of those genes are known to cause muscular dystrophies (Savarese et al., 2016; Vainzof et al., 2008). In this study, we investigated whether SFPQ-dependent machinery for long genes expression is also essential for muscle cells, what is the regulatory target genes and physiological functions in skeletal muscle, and also whether dysregulations of long genes could cause disorders in muscle functions or diseases. Here we show that loss of *Sfpq* disturbed extra-long gene expression, indicating the significance of SFPQ for the full-length transcription of extra-long genes not only in the nervous system but also in muscle cells. Phenotypically, skeletal-muscle-specific disruption of *Sfpq* caused progressive muscle mass reduction. Mechanistically, SFPQ regulates the expression of multiple metabolic pathway genes that are identified by functional clustering analysis. Our results show that SFPQ-dependent transcriptional regulation of extra-long genes is required in muscle tissue and SFPQ

[1]Department of Anatomy and Developmental Biology, Graduate School of Medicine, Kyoto University, Sakyo-ku, Kyoto 606-8501, Japan

[2]Department of Molecular Therapy, National Institute of Neuroscience, National Center of Neurology and Psychiatry, Kodaira, Tokyo 187-8502, Japan

[3]Department of Cell Physiology, The Jikei University School of Medicine, Minato-ku, Tokyo 105-8461, Japan

[4]Medical Research Support Center, Graduate School of Medicine, Kyoto University, Sakyo-ku, Kyoto 606-8501, Japan

[5]Lead Contact

*Correspondence: takeuchi.akihide.8r@kyoto-u.ac.jp (A.T.), hagiwara.masatoshi.8c@kyoto-u.ac.jp (M.H.)

https://doi.org/10.1016/j.isci.2019.02.023

plays crucial roles to regulate muscle-specific target genes essential for the energy metabolism and to maintain muscle mass.

RESULTS

Loss of *Sfpq* Caused Severe Growth Defect

To elucidate whether SFPQ regulates muscle long genes and what the physiological role(s) of SFPQ is in skeletal muscle *in vivo*, we developed conditional gene-knockout (KO) mice for *Sfpq*. As *Sfpq*-null mutant mice in whole body caused early embryonic lethality (Takeuchi et al., 2018), we selectively deleted *Sfpq* gene in skeletal muscle by crossing *Sfpq*-floxed mice (*Sfpq*$^{f/f}$) with *Mlc1f-Cre* transgenic mice. *Mlc1f-Cre* mice express Cre recombinase under the control of the *myosin light chain* (*Mlc*)*1f* promoter, which selectively expresses Cre in skeletal muscle except heart and thus enables us to analyze the physiological functions of SFPQ in skeletal muscle eliminating heart-related symptoms (Bothe et al., 2000). Homozygous KO mice (*Sfpq*$^{f/f}$*;Mlc1f-Cre*) (KO mice) were born at the expected Mendelian ratios (Figure S1A) and were indistinguishable from littermates control mice, indicating that loss of *Sfpq* did not cause detectable abnormalities during the embryonic period. We next monitored the growth of KO mice during the postnatal period. Total body weight and appearance were indistinguishable from those of control mice until postnatal day 14 (P14). However, KO mice started to show a marked and progressing reduction in body weight around P16 relative to their littermate controls, whereas the body weight of heterozygous (*Sfpq*$^{f/+}$*;Mlc1f-Cre*) mice did not differ from that of littermate controls (Figure 1A). KO mice caused sudden death starting from P33, and all of them had died by P50 (Figure 1B). KO mice showed smaller body size and pronounced kyphosis, which became evident around P30, the typical phenotypes frequently observed in association with muscle weakness (Figure 1C). Given that loss of *Sfpq* caused quite severe growth defects throughout the body with premature death, we examined whether KO mice selectively disrupted *Sfpq* gene only in skeletal muscle tissue using genomic PCR targeting the floxed allele of *Sfpq*. In KO mice, deletion of *Sfpq* gene was detected in all skeletal muscles examined, including the diaphragm (DIA), gastrocnemius (GC), tibialis anterior (TA), and soleus (SOL), but not in the heart, brain, liver, kidney, or spleen, confirming that observed systemic phenotype is originated from the skeletal muscle-specific disruption of the *Sfpq* gene (Figure S1B; KO allele). As we found remaining weak band from floxed alleles in skeletal muscle tissues (Figure S1B; floxed allele), we histologically accessed muscle-specific disruption of *Sfpq* in KO mice. SFPQ expression in myofibers was detected in nuclei that attach to the inside of the sarcolemma (Laminin2 positive plasma membrane of myofiber) as observed in control GC, TA, and SOL muscles (Figures S1C and S1D, open arrow heads). We also detected accumulation of nuclei in the fibroblasts or vascular cells in connective tissue between myofibers that are negative for laminin (Figure S1C, Control-GC). In KO mice, we found selective loss of SFPQ staining in the nuclei of myofibers of GC muscles with remaining expression of SFPQ in the connective tissues (Figure S1C, KO-GC), suggesting that *Mlc1f-Cre* mice efficiently disrupted SFPQ expression selectively in skeletal muscle cells by P30. From these observations, we confirmed that severe growth abnormalities and premature death were caused by the selective disruption of *Sfpq* in skeletal muscle tissues. Since Cre expression under the control of *Mlc1f* promoter is restricted to fast fibers (Mourkioti et al., 2008; Schiaffino and Reggiani, 1994), we examined whether efficiency of Cre excision is different between slow-twitch (SOL) and fast-twitch (TA) muscles. We observed SFPQ-positive nuclei in SOL in KO mice by immunostaining (Figure S1D, upper panels, open arrow heads in KO-SOL), indicating remaining expression of SFPQ. Furthermore, expression level of SFPQ protein was confirmed by western blotting (WB) (Figure S1D, lower panel, fold change [FC] for KO/Ct: 0.46 [TA] and 0.66 [SOL]), indicating the difference of SFPQ disruption between slow-twitch and fast-twitch muscles. These results are consistent with the previous report generating and characterizing *Mlc1f-Cre* mice (Bothe et al., 2000; Mourkioti et al., 2008; Patel et al., 2008), indicating that Cre excision is rather weak in slow-twitch muscle and intact in non-myogenic cells such as fibroblasts, Schwann cells, and satellite cells contained in skeletal muscle tissues, thus caused remaining weak band from floxed alleles in entire skeletal muscle tissues in genotype PCR.

Sfpq KO Mice Exhibited Reduced Muscle Mass

To further characterize skeletal muscle abnormalities in KO mice, muscle tissues were morphologically analyzed. At 1 month old (P30), the average body weight in KO mice was significantly reduced to 55% of that in littermate controls (Figure 1D, left bar graph). Accordingly, the mass of various types of skeletal muscles, including fast-twitch glycolytic muscles such as TA and GC, slow-twitch oxidative muscles such as SOL, and also mixed-fiber muscle of DIA, was about 45% lower in KO mice than in controls (Figure 1D, right bar graphs). As KO mice showed smaller body size than controls (Figure S1E), we examined whether loss of

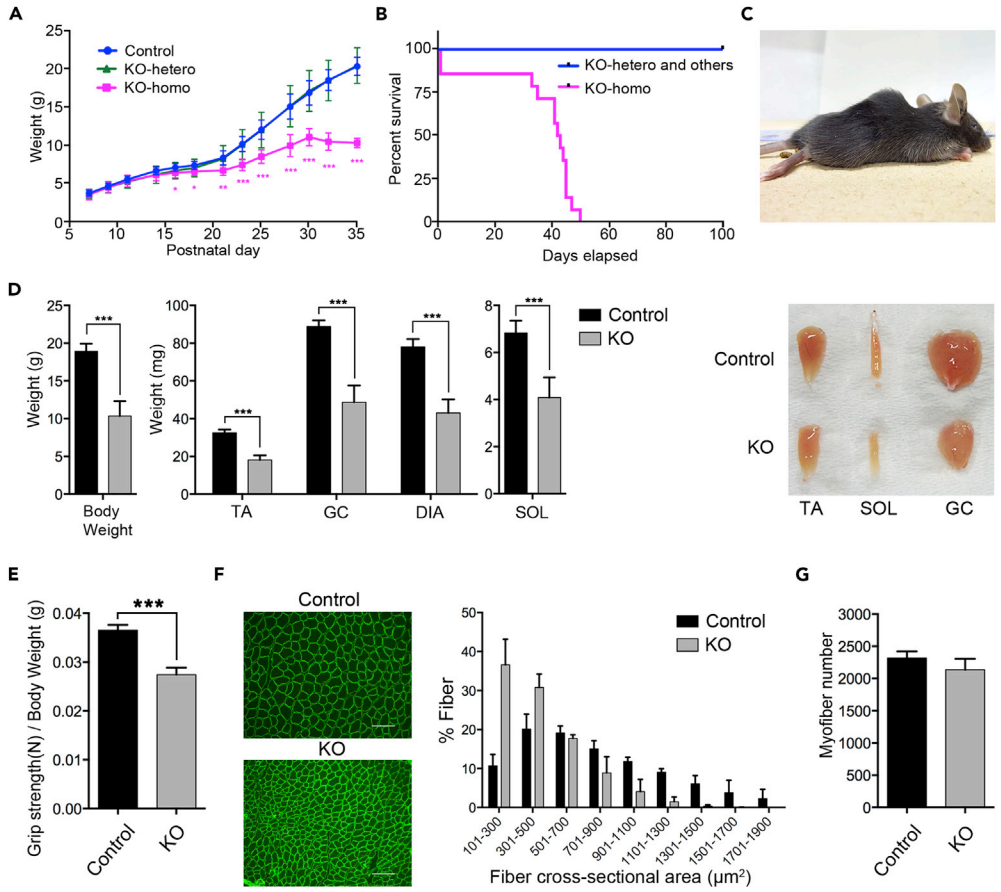

Figure 1. *Sfpq* Mutants Exhibit Skeletal Muscle Growth Defects with Kyphosis and Premature Death

(A) Growth charts of male skeletal muscle-specific *Sfpq* homozygous knockout mice (KO-homo) (n = 4), heterozygous knockout mice (KO-hetero) (n = 7), and littermate control mice (n = 16). Data are presented as mean ± SD. *p < 0.05, **p < 0.01, ***p < 0.001 versus control (Student's or Welch's t test).

(B) Kaplan-Meier survival curves for male and female KO-homo (n = 14) and control (KO-hetero and others) (n = 27) mice.

(C) Kyphosis phenotype observed in P35 male KO mice.

(D) Body weight and weight of various skeletal muscles in male KO and control mice (n = 5). Representative skeletal muscle samples from KO and control mice (*right*). DIA, diaphragm; GC, gastrocnemius; SOL, soleus; TA, tibialis anterior. Data are presented as mean ± SD. ***p < 0.001 (Student's test).

(E) Grip strength test performance normalized to body weight of male KO (n = 19) and control (n = 20) mice from P26 to P30. Data are presented as mean ± SEM. ***p < 0.001 (Student's t test).

(F) Cross-section of laminin-stained TA muscle from 1-month-old male KO and control mice (*left*). Scale bars: 100 μm. Histogram of cross-sectional area (μm^2) of laminin-stained myofibers from KO and control mice (*right*) (n = 3). Data are presented as mean ± SD. The difference of the distribution of cross-sectional area between KO and control mice was statistically significant (p < 0.001) (totally nine sections from three mice in each genotypes) using Mann-Whitney U test.

(G) Number of myofibers in TA muscle from 1-month-old male KO and control mice (n = 3, totally three sections from three mice in each genotype). Data are presented as mean ± SEM. There was no significant difference with Student's t test.

See also Figure S1.

Sfpq caused systemic growth arrest by analyzing morphology of bone and brain. The length of long bones, such as the tibia, and the size and shape of the skull bone and brain was indistinguishable between KO mice and their littermate controls (Figure S1F), indicating that growth-hormone-dependent skeletal development was intact in KO mice. Instead, all KO mice exhibited growing pronounced kyphosis during development, which made the mice look smaller (Figure 1C).

Next, we assessed the muscle function in KO mice by several behavioral examinations. The grip-strength test was conducted to examine the muscle strength of forelegs. As the body weight in KO mice was relatively smaller than in control mice (Figure 1A), we evaluated the muscle strength by calculating force per

body weight (Connolly et al., 2001). The grip strength per body weight of KO mice was significantly lower than that of controls (FC = 0.75; Figure 1E). We further examined the muscle force with endurance and motor skill by the hanging wire and the rotarod tests. Muscle strength and motor function in KO mice were significantly decreased with these tests (Figures S1G and S1H), indicating that loss of *Sfpq* caused muscle mass reduction with significant impairment of motor function.

To further investigate the cause of severe muscle mass reduction and impairment of motor function, we examined the number and size of myofiber using quantitative analysis of the cross-sectional area in TA muscle. The size of each myofiber was significantly reduced in KO compared with that in control mice (Figure 1F). When we counted the number of total myofibers in TA muscle samples, there was no difference with the myofiber number itself between KO and control mice (Figure 1G). Since the total number of myofibers is defined during the embryonic period and myofiber size is developed during the postnatal periods, it is indicated that loss of *Sfpq* does not affect myofiber generation but reduces the size of each myofiber, resulting in an overall decrease in body weight after P14.

Loss of *Sfpq* in Skeletal Muscle Causes Metabolic Myopathy but Not Typical Dystrophic Phenotypes

To elucidate the pathogenesis of *Sfpq* disruption to cause severe muscle mass reduction, histological analyses were conducted using standard H&E staining. Given that SFPQ is essential for regulating the transcription of extra-long genes in neural tissue (Takeuchi et al., 2018), it could be expected that loss of *Sfpq* disrupts the expression of long genes including *Dmd* in KO mice, which causes muscular dystrophy. Then we examined sections of TA and DIA muscles from KO mice from P14 to P30 (from starting point of body weight loss and before sudden death); however, H&E sections of TA and DIA muscles from P30 KO were indistinguishable from those in control mice except for the smaller fiber size observed in KO mice samples (Figure 2A). We could not detect any symptoms of myofiber degeneration such as inflammation and neutrophil infiltration, regeneration with centrally located myonuclei, fiber splitting, or replacement of myofibers with connective tissues. This result indicated that severe muscle mass reduction in KO mice was not caused as the symptoms of muscular dystrophy. A series of histopathological analyses was further conducted to characterize the observed myopathy in KO mice. In nicotinamide adenine dinucleotide-tetrazolium reductase (NADH-TR) and modified Gomori trichrome staining, no obvious irregular intermyofibrillar network and abnormal aggregates, such as "raggedred" and "moth-eaten" fibers, were detected in the TA muscle sections from 1-month-old KO mice. However, myofibers that are rather densely stained with modified Gomori trichrome staining in TA muscle of KO mice were increased in number, indicating the increment in the proportion of oxidative fibers (Figure 2B, Gomori). The intensity with NADH-TR staining became weaker in TA muscle of KO mice, indicating the decrease of NADH dehydrogenase activity in mitochondria complex I (Figure 2B, NADH-TR). The result of Gomori trichrome staining suggests the possibility that loss of *Sfpq* caused fiber type change. Thus, we analyzed and quantified fiber type distribution using immunohistochemistry for myosin heavy chain (MyHC) expression. The number of MyHC I and IIA-positive fibers in the TA muscle was 4% and 26% higher, respectively, whereas the number of MyHC IIB-positive fibers was 10% lower in 1-month-old KO mice compared with those in control littermates (Figure 2C). Given that fibers expressing MyHC I and IIA have greater oxidative capacity than those expressing MyHC IIB, these findings indicate that loss of *Sfpq* induced a shift toward more oxidative fiber types, which is a well-observed phenomenon in myopathies. We further examined the amount of mitochondrial oxidative phosphorylation (OXPHOS) complexes from the observation of lower NADH dehydrogenase activity in mitochondria complex I of TA muscles in KO mice (Figure 2B). Then we found significant decreases in the abundance of OXPHOS complex I (35%), complex II (18%), and complex IV (35%) in TA muscle in KO relative to those in control mice (Figure 2D). We next examined the glycogen accumulation using periodic acid Schiff staining. Surprisingly, glycogen in entire GC muscle in KO was more intensively stained than that in control mice, indicating that loss of *Sfpq* caused excess glycogen accumulation (Figure 2E). We quantified the amount of glycogen content in GC muscle and found a 2.5-fold increase in KO compared with that in control mice (Figure 2F). Together, loss of *Sfpq* caused decreased OXPHOS complexes in mitochondria; in the meantime, excess glycogen was accumulated in skeletal muscles, indicating features of metabolic myopathy.

Loss of *Sfpq* Specifically Downregulated Long Genes in Muscle Cells

We next tried to investigate whether SFPQ regulates specific target long genes in muscles using transcriptome study. Histological analyses revealed that the size of each myofiber was significantly reduced in KO

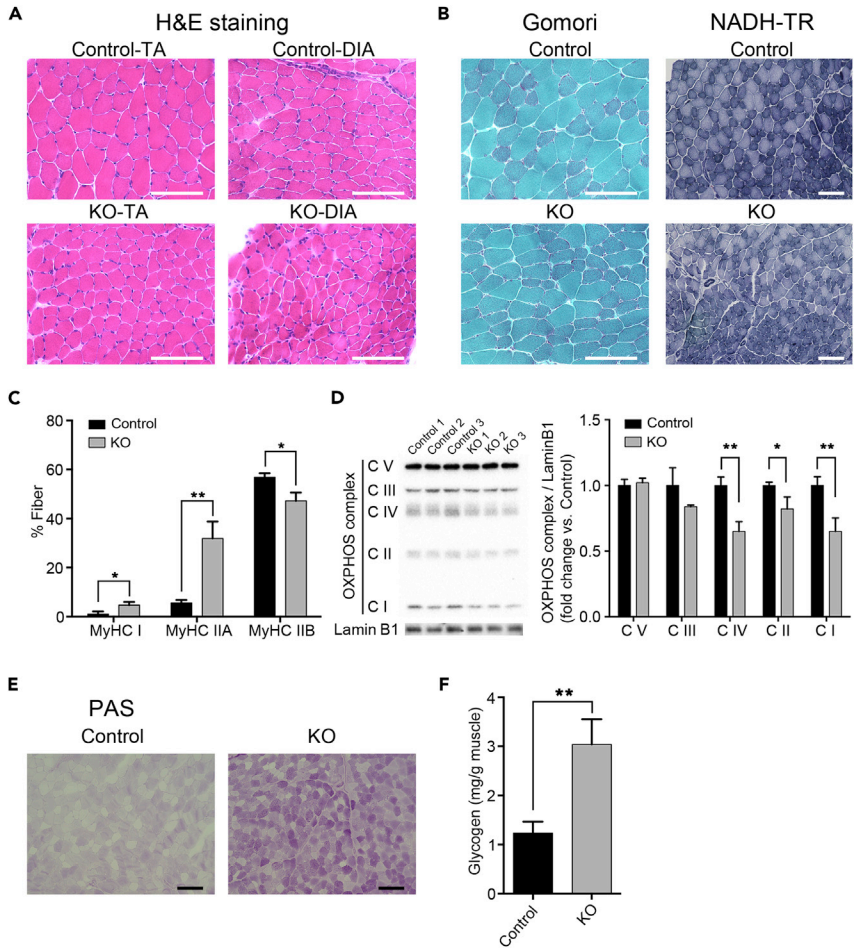

Figure 2. Loss of *Sfpq* in Skeletal Muscle Causes Metabolic Myopathy but Not Typical Dystrophic Phenotypes

(A and B) (A) Representative cross-section of H&E-stained TA muscle from 1-month-old male KO and control mice. Scale bars: 100 μm. (B) Representative cross-section of modified Gomori trichrome stained TA muscle from 1-month-old male KO and control mice. Scale bars: 100 μm (*left*). Representative cross-section of NADH-TR stained TA muscle from 1-month-old male KO and control mice. Scale bars: 100 μm (*right*).

(C) Percentage distribution of MyHC isoforms I, IIA, and IIB in TA muscle of male KO and control mice ($n = 3$, totally three sections from three mice in each genotype). Data are presented as mean ± SD. *$p < 0.05$, **$p < 0.01$ (Student's t test).

(D) Representative results of WB using an OXPHOS antibody cocktail on TA muscle samples from male KO and control mice. Lamin B1 was used as a loading control. Signal intensities were quantified by densitometry ($n = 3$). CI, complex I (Ndufb8); CII, complex II (Sdhb); CIII, complex III (Uqcrc2); CIV, complex IV (mt-Co1); and CV, complex V (Atp5a1). Data are presented as mean ± SD. *$p < 0.05$, **$p < 0.01$ (Student's or Welch's t test).

(E) Representative periodic acid Schiff staining of GC sections from 1-month-old male KO and control mice. Scale bars: 100 μm.

(F) Glycogen content in GC muscles from 1-month-old male KO and control mice ($n = 3$). Data are presented as mean ± SD. **$p < 0.01$ (Student's t test).

mice and the relative amount of connective tissue and non-myogenic cells contained in muscle was much higher in KO than in control mice (Figure 1F). To eliminate the contamination of non-muscle cells in the transcriptome study, we decided to use primary myotubes isolated from KO and control mice for RNA sequencing (RNA-seq). We raised primary myoblasts from 1-month-old KO and control mice, induced differentiation into myotubes, and extracted total RNA for RNA-seq. SFPQ protein levels in *Sfpq*$^{-/-}$ myotubes (KO myotubes) were confirmed as ~35% compared with control myotubes by WB, indicating that differentiation-induced Cre expression successfully disrupted *Sfpq* gene and decreased its protein level in KO myotubes (Figure S2A). Similarly, *in vivo*, we histologically examined SFPQ disruption in myotube and confirmed that SFPQ expression is selectively downregulated in the nuclei of MyHC-positive differentiated

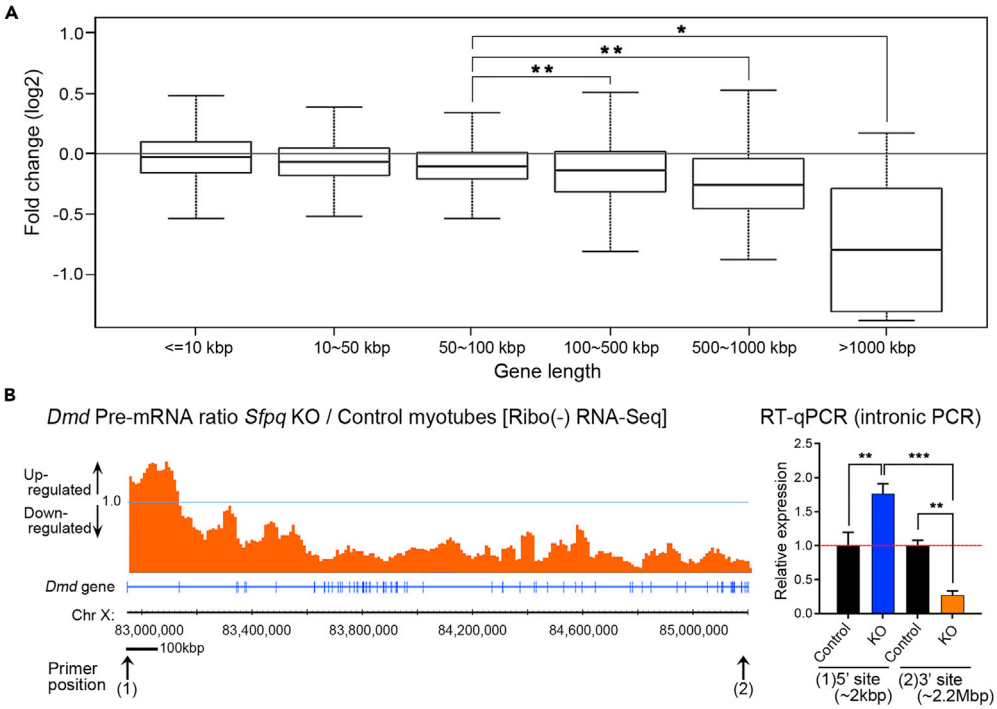

C

KEGG gene sets downregurated in KO myotubes

Rank	Gene set	NES	NOM *P* value	FDR *q* value
1	PYRUVATE_METABOLISM	-2.404	0.000***	0.000***
2	PROPANOATE_METABOLISM	-2.286	0.000***	0.000***
3	CITRATE_CYCLE_TCA_CYCLE	-2.079	0.000***	0.000***
4	VALINE_LEUCINE_AND_ISOLEUCINE_DEGRADATION	-2.036	0.000***	0.000***
5	GLYCOLYSIS_GLUCONEOGENESIS	-1.987	0.000***	0.000***
6	STARCH_AND_SUCROSE_METABOLISM	-1.934	0.000***	0.001**
7	FATTY_ACID_METABOLISM	-1.924	0.000***	0.001**
8	TRYPTOPHAN_METABOLISM	-1.850	0.000***	0.004**
9	OXIDATIVE_PHOSPHORYLATION	-1.843	0.000***	0.004**
10	FRUCTOSE_AND_MANNOSE_METABOLISM	-1.843	0.001**	0.004**
11	ALZHEIMERS_DISEASE	-1.829	0.000***	0.004**
12	BUTANOATE_METABOLISM	-1.793	0.000***	0.007**
13	PENTOSE_PHOSPHATE_PATHWAY	-1.786	0.001**	0.008**
14	METABOLIC_PATHWAYS	-1.764	0.000***	0.000***
15	PARKINSONS_DISEASE	-1.762	0.000***	0.010**

D

REACTOME gene sets downregulated in KO myotues

Rank	Gene set	NES	NOM *P* value	FDR *q* value
1	GLUCOSE_METABOLISM	-2.218	0.000***	0.000***
2	TCA_CYCLE_AND_RESPIRATORY_ELECTRON_TRANSPORT	-2.192	0.000***	0.001**
3	PYRUVATE_METABOLISM_AND_CITRIC_ACID_TCA_CYCLE	-2.154	0.000***	0.000***
4	GLUCONEOGENESIS	-2.057	0.000***	0.001**
5	RESPIRATORY_ELECTRON_TRANSPORT_ATP_SYNTHESIS_BY_CHEMIOSMOTIC_COUPLING_AND_HEAT_PRODUCTION_BY_UNCOUPLING_PROTEINS	-2.003	0.000***	0.001**
6	PYRUVATE_METABOLISM	-1.974	0.000***	0.002**
7	METABOLISM_OF_CARBOHYDRATES	-1.908	0.000***	0.006**
8	RESPIRATORY_ELECTRON_TRANSPORT	-1.900	0.000***	0.005**
9	CITRIC_ACID_CYCLE_TCA_CYCLE	-1.885	0.000***	0.005**

Figure 3. *Sfpq* Deficiency Inhibits the Expression of Extra-Long Genes and the Metabolism-Related Gene Expression

(A) Box plots showing changes in gene expression in KO myotubes relative to control myotubes. Bins were defined according to gene length. *p < 0.01, **p < 0.001 for changes between two bins (Mann-Whitney U test).

(B) Pre-mRNA ratio of *Dmd* calculated by pre-mRNA levels in KO vs. control myotubes using Ribo(−) RNA-seq data (*left*) and the result of RT-qPCR for *Dmd* pre-mRNA between KO and control myotubes at the indicated positions ($n = 3$) (*right*). Data are presented as mean ± SD. **p < 0.01, ***p < 0.001 (Student's t test).

(C and D) List of significantly downregulated gene sets identified by GSEA analysis using KEGG (C) and Reactome (D) gene sets in KO as compared with control myotubes. Rank is based on the normalized enrichment score (NES) of each pathway. Gene sets ($q < 0.01$) are listed. FDR, false discovery rate; NOM, nominal. **p, $q < 0.01$, ***p, $q < 0.001$ (permutation test).

See also Figures S2–S4.

myotubes from *Sfpq*-KO mice (Figure S2B). In RNA-seq analysis using polyA-selected mRNAs for mature mRNA expression, observed gene expression changes between KO and control myotubes were quite small among 10,810 expressed genes (transcripts per million [TPM] ≥ 2.0 in either KO or control myotubes) (Figure S2C), which is consistent with our previous observation that SFPQ regulates limited numbers of target extra-long genes in embryonic mouse brains (Takeuchi et al., 2018). To see whether SFPQ specifically regulates long genes similarly in muscle, we examined the relationship between FC with pre-mRNA length of expressed genes. As gene length increased from 100 kbp and beyond, the FC in KO myotubes tended to be more negative (Figure 3A; median FC = 0.89 for genes 100–500 kbp, 0.79 for genes 500–1,000 kbp, and 0.59 for genes >1,000 kbp), indicating extra-long gene-specific downregulation. In brain, SFPQ-regulated genes caused gradual downregulation of pre-mRNAs when *Sfpq* is disrupted owing to the impairment of transcriptional elongation (Takeuchi et al., 2018). We next examined whether downregulated long genes in KO myotubes show this typical gradual downregulation by RNA-seq using rRNA depleted total RNAs for pre-mRNAs [RNA-Seq Ribo(−)]. For *Dmd* genes, pre-mRNA level was not downregulated or rather upregulated in the 5′ region (ratio >1.0) but decreased beyond the middle of the transcript close to 5′ region (ratio <1.0) and plateaued out to the 3′ end (Figure 3B, left panel). We further confirmed that the pre-mRNA ratio (KO/Control) of the 3′ site was significantly lower than that of the 5′ site using reverse transcriptase-quantitative PCR (RT-qPCR) (hereinafter called "3′-site downregulation"), indicating the impairment of transcriptional elongation of *Dmd* gene (Figure 3B, right panel). These results indicate that *Sfpq* is an essential regulator of transcriptional elongation of extra-long genes such as *Dmd* in skeletal muscle.

Sfpq Regulates Energy Metabolism Pathway Genes in Muscle Cells

In our histological analyses, KO mice did not show typical dystrophic phenotypes (Figure 2A). We examined the mature mRNA level of *Dmd* gene in GC muscles (P35) using RT-PCR and found that the *Dmd* mRNA level in KO was about 25% of that in control mice (FC = 0.25 vs. control mice, data not shown). As 25% of expression is still not critically low for causing muscular dystrophy, this can be the explanation why KO mice did not exhibit phenotypes that are typically observed in *Dmd* mutant mice (Vainzof et al., 2008; van Putten et al., 2012). Recent studies and our own have indicated that RBPs regulate functional clusters of genes known as regulons (Cosker et al., 2016; Keene, 2007; Takeuchi et al., 2018). To identify SFPQ regulons in skeletal muscle, gene set enrichment analysis (GSEA) was performed (Subramanian et al., 2005) using gene sets from the Kyoto Encyclopedia of Genes and Genomes (KEGG) and Reactome platforms (Kanehisa and Goto, 2000; Matthews et al., 2009). Gene sets significantly up- or downregulated in KO myotubes were identified using FDR (false discovery rate), or q values <0.01. In significantly downregulated genes, 15 and 9 pathways were identified using the KEGG and Reactome platforms, respectively. Surprisingly, 13 of the 15 downregulated gene sets in KEGG exclusively comprised metabolism-related gene clusters encompassing the tricarboxylic acid (TCA) cycle, pyruvate metabolism, OXPHOS, gluconeogenesis, and fatty acid metabolism, with the other two sets relating to Parkinson and Alzheimer diseases, which include mitochondria-related genes (Figures 3C and S2D). The nine downregulated gene sets enriched in Reactome comprised metabolism-related gene clusters relating to gluconeogenesis, glucose metabolism, TCA cycle, or respiratory electron transport (Figures 3D and S2D). Significantly upregulated gene sets were also identified using KEGG or Reactome, but none of them has a clear relation with muscle mass reduction (data not shown). Together, it is suggested that SFPQ regulates a wide range of energy metabolism pathway gene expression, and loss of *Sfpq* disturbed metabolic regulation leading to severe muscle mass reduction in KO mice.

Next, we focused individual downregulated genes in energy metabolism pathways. Using the threshold of FC < 0.769 (1/1.3) and q value <0.1 in all expressed genes (TPM ≥2), totally 32 genes were identified as

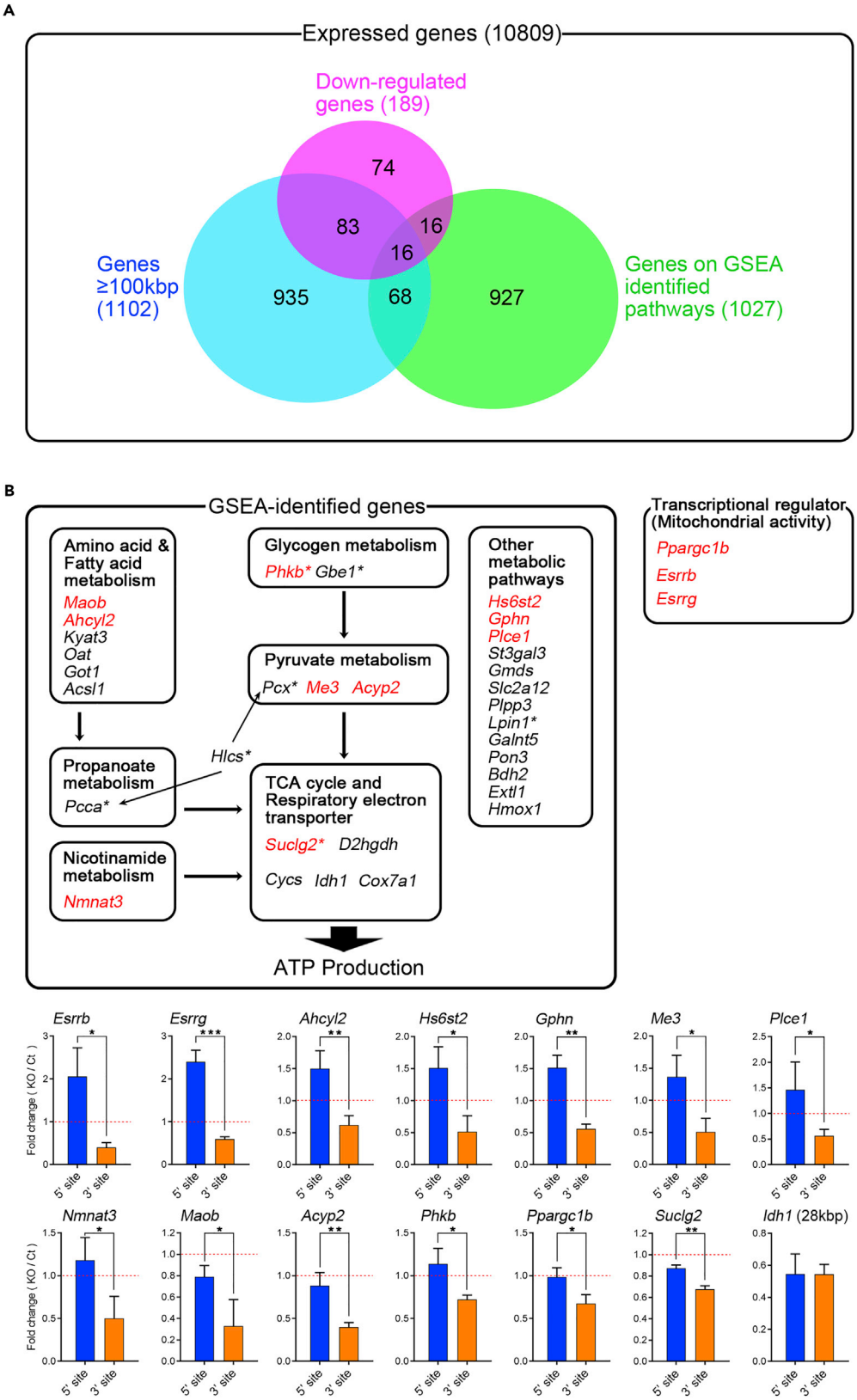
A
Expressed genes (10809)
Down-regulated genes (189)
74
83
16
16
Genes ≥100kbp (1102)
935
68
927
Genes on GSEA identified pathways (1027)
B
GSEA-identified genes
Amino acid & Fatty acid metabolism
Maob
Ahcyl2
Kyat3
Oat
Got1
Acsl1
Glycogen metabolism
Phkb* Gbe1*
Pyruvate metabolism
Pcx* Me3 Acyp2
Hlcs*
Propanoate metabolism
Pcca*
TCA cycle and Respiratory electron transporter
Suclg2* D2hgdh
Cycs Idh1 Cox7a1
Nicotinamide metabolism
Nmnat3
ATP Production
Other metabolic pathways
Hs6st2
Gphn
Plce1
St3gal3
Gmds
Slc2a12
Plpp3
Lpin1*
Galnt5
Pon3
Bdh2
Extl1
Hmox1
Transcriptional regulator (Mitochondrial activity)
Ppargc1b
Esrrb
Esrrg
Esrrb
Esrrg
Ahcyl2
Hs6st2
Gphn
Me3
Plce1
Nmnat3
Maob
Acyp2
Phkb
Ppargc1b
Suclg2
Idh1 (28kbp)
Fold change (KO / Ct)
5' site
3' site

Figure 4. Loss of *Sfpq* Downregulates Energy Metabolism Pathway Gene Expression in Muscle Cells

(A) Venn diagram of downregulated genes, genes≥100 kbp, and genes on GSEA identified pathways.

(B) Upper panel: Schematic diagram of downregulated genes in KO myotubes, which are GSEA-identified metabolic-pathway-related genes and also transcriptional regulators for mitochondrial activity. Asterisk indicates HGMD-identified inherited metabolic-diseases-related genes in Figure S2E. Lower panel: RT-qPCR for 5′ and 3′ sites of pre-mRNAs ($n = 3$). Pre-mRNA ratio (fold change) was calculated between KO and control myotubes for each position (Control = 1). *Idh1* gene was used as negative control (the gene length <100 kbp). Genes showing 3′-site downregulation are highlighted with red characters in upper panel. Data are presented as mean ± SD. *p < 0.05, **p < 0.01, ***p < 0.001 (Student's or Welch's t test).

See also Figures S2–S4.

significantly downregulated genes in GSEA, and 16 (50%) among them are longer than 100 kbp (Table S1). On the other hand, 1,027 genes were included in entire GSEA among expressed genes, however only 84 of them were longer than 100 kbp (8.2%) (Figure 4A), indicating that downregulated genes in GSEA are significantly enriched long gene >100 kbp as SFPQ target genes. We also found that 11 long genes were involved in pathways related to ATP production, i.e., glycogen, pyruvate, fatty acid, amino acid, and mitochondrial metabolism (Figure 4B and Table S1). Of the downregulated long genes longer than 100 kbp but not included in the GSEA-identified gene sets, three genes related to ATP production were significantly downregulated in KO relative to control myotubes; these encoded transcriptional regulators of mitochondria and oxidative metabolism (*Ppargc1b* [*peroxisome proliferative activated receptor, gamma, coactivator 1 beta*] [*PGC1β*]: 102 kbp, FC = 0.73, p < 0.01; *Esrrb* [*estrogen-related receptor β*]: 161 kbp, FC = 0.39, p < 0.001; and *Esrrg* [*estrogen-related receptor γ*]: 217 kbp, FC = 0.52, p < 0.001). Loss of *PGC-1α/β* and *estrogen-related receptors* (*Esrrs*) decreased mitochondrial OXPHOS complexes or changed the slow- or fast-myofiber type distribution (Gan et al., 2013; Gudiksen and Pilegaard, 2017; Zechner et al., 2010) as similarly observed in *Sfpq*-KO mice. To identify SFPQ target genes, we examined the pre-mRNA level of the downregulated metabolic pathway relating long genes (genes in Figure 4B, upper panel) in a similar way with *Dmd* gene using RT-qPCR (Figure 3B). Thirteen genes showing 3′-site downregulation were identified as SFPQ target genes (Figure 4B, lower panel) and highlighted with red characters (Figure 4B, upper panel). These results indicated that SFPQ is broadly involved in metabolic pathway regulations of skeletal muscle. Of 32 downregulated genes in GSEA in upper panel of Figure 4B, 7 were associated with inherited metabolic diseases according to the Human Gene Mutation Database (HGMD), and *Phkb* (*phosphorylase kinase beta*) and *Suclg2* (*succinate-Coenzyme A ligase, GDP-forming, beta subunit*) are identified as SFPQ target genes (Figure 4B, lower panel, Figure S2E). *Phkb* is known as the causative gene for glycogen storage disease type IX (Beauchamp et al., 2007; Burwinkel et al., 1997) that is consistent with our observations of increased glycogen accumulation of GC muscle in KO mice (Figures 2E and 2F).

Next, we confirmed downregulation of long genes and metabolic pathway genes *in vivo* using RNA-seq analysis in GC muscles from P35 male KO and control mice. First, the relationship between FC with pre-mRNA length of expressed genes were similarly analyzed *in vitro*. As gene length increased from 100 kbp and beyond, the FC tended to be more negative in KO GC muscle (Figure S3A), indicating long-gene transcriptopathy. We further examined mRNA expression changes of long genes relating to energy metabolism pathways that were identified *in vitro* and confirmed well-overlapped downregulated genes *in vivo* with *in vitro* (Figure S3B). Using RT-qPCR and WB, we validated the downregulation of mRNA and proteins of SFPQ target genes *in vivo* for the representative genes (*Phkb*, *Me3* [*malic enzyme 3, NADP(+)-dependent, mitochondrial*], and *Gphn* [*gephyrin*]) (Figures S3C and S3D). These results indicated that metabolic-pathway-related genes were downregulated *in vivo*. We further assessed systemic energy metabolism by measuring blood glucose concentration in KO mice. In fasted condition, the blood glucose level was significantly lower in KO mice than in control mice (Figure S3E), indicating that loss of *Sfpq* impaired energy metabolism regulation in skeletal muscle, presumably increased glucose uptake, and further affected systemic energy regulation. This lower glucose level in KO mice potentially worsens muscle mass reduction and could be the cause of premature death.

We next tried to access why loss of *Sfpq* caused severe muscle mass reduction in KO mice. First, we examined the possibility of catabolic pathway activation (protein degradation pathway). We checked the mRNA expression of 18 genes relating to Ubiqutin-Proteasome, Calpine-Calpastatin, and Lysosome-Autophagy system (Carmignac et al., 2011; Stefanetti et al., 2015; Tipton et al., 2018; Yamamoto et al., 2015). There was limited upregulation only in *Ctsl* (*Cathepsin L*) (FC = 1.44), but the expression of all other genes was

comparable between KO and control muscle (Figure S4A). In addition, we considered the possibility of dysfunction in anabolic pathway (protein synthesis). We examined protein synthesis in KO muscle by the surface sensing of translation (SUnSET) technique (Goodman et al., 2011). There was no significant reduction of puromycin-labeled peptides in KO muscle compared with controls, indicating that protein synthesis was not significantly impaired in KO muscles (Figure S4B). Together, it is indicated that both catabolic and anabolic pathways were not disturbed as the cause of severe muscle mass reduction in KO mice.

For further evaluation of muscle growth defect in KO mice, we determined the correlation between *Sfpq* and its target metabolic pathway relating genes during postnatal muscle development (P2, P7, P14, P21, and P28) in wild-type mice. Only modest change in the level of *Sfpq* mRNA was detected during postnatal muscle development, whereas that of all target genes except *Plce1* and *Hs6st2* were comprehensively upregulated during P14 to P28 (Figure S4C), consistent with our observation that body weight reduction in KO mice became evident in this stage. These results suggest that SFPQ is critically required for the upregulation of metabolic pathway genes and the muscle growth from P14.

DISCUSSION

In this study, we found that skeletal muscle-specific disruption of *Sfpq* inhibited the expression of extra-long genes, indicating that SFPQ-dependent machinery is generally crucial for the full-length transcription of extra-long genes in muscle cells as we observed in the nervous system. We initially expected that extra-long genes such as *Ttn*, *nebulin*, *Dysf*, *laminin α2*, and *Sgcd* that are related to skeletal muscle structure or muscular dystrophy would be downregulated in KO mice, but this was not the case. Thus, *Sfpq* regulation does not extend to all long genes. In the developing brain, SFPQ regulates fewer than 10% of expressed long genes >100 kbp in length; a Gene Ontology analysis showed that target genes are related to neuronal development and maturation (Takeuchi et al., 2018). In skeletal muscle, we found that downregulated genes in KO myotube were highly enriched in metabolism such as glucose metabolism, TCA cycle, and respiratory electron transport indicating energy metabolism pathways as regulons of SFPQ. These results indicate that SFPQ specifically regulates tissue-specific target genes and is essential for regulating energy metabolism in skeletal muscle, which is closely related to the maintenance of muscle mass and motor function (Cunningham et al., 2007; Laplante and Sabatini, 2012; Mouisel et al., 2014). In addition, a recent study demonstrated that disruption of splicing factors *Rbfox1* and *Rbfox2* caused severe loss of muscle mass (Singh et al., 2018), indicating that RBPs are essential for the maintaining muscle mass as we observed in *Sfpq*-KO mice.

Energy metabolism in muscle is classified into two distinct energy-supplying systems: anaerobic metabolism, which provides energy from glycogenolysis/glycolysis for rapid movements, and aerobic metabolism, regulated by mitochondria for sustained exercise (Zierath and Hawley, 2004). The dependency on two energy-supplying systems are flexibly changed and compensated with each other for adapting to the energy requirement status such as exercises, whereas dysregulation of energy metabolism is associated with muscle mass reduction and dysfunction in pathophysiological conditions such as aging (sarcopenia), chronic diseases (cachexia), and atrophy of the other origin (Brocca et al., 2012; Carson et al., 2016; Dirks et al., 2006). Actn3 (Actinin alpha 3) is essential for glycogenolysis by activating glycogen phosphorylase. In *Actn3*-KO mice, glycogen conversion to glucose is impaired and glycogen accumulates in muscle, resulting in a slight reduction in muscle mass and decreased body weight (MacArthur et al., 2008; Quinlan et al., 2010), similar to what is observed in *Sfpq*-KO mice.

Regulation of energy metabolism is closely related to the maintenance of muscle mass and motor function and involves factors such as myostatin as well as IGF1-AKT-mTOR (insulin-like growth factor 1-AKT-mechanistic target of rapamycin) signaling pathway and its downstream transcriptional regulators PGC-1α and -1β (Cunningham et al., 2007; Laplante and Sabatini, 2012; Mouisel et al., 2014). For aerobic ATP production in mitochondria, PGC-1α and -1β play essential roles in coordinately activating nuclear and mitochondrial genes. Yy1 (Yin yang 1) is a transcription factor modulated by PGC-1α that regulates mitochondrial biogenesis. Skeletal-muscle-specific *Yy1*-knockout mice show decreases in mitochondrial OXPHOS complexes and have a dwarf-like appearance. Surprisingly, identified pathways downregulated in the skeletal muscles of *Sfpq*-KO mice well overlapped to those in *Yy1*-KO mice, indicating that genes regulating mitochondrial metabolism are synergistically regulated by transcription factor and RBP. Major differences in these two KO mice is that glycogenolysis was unaffected in *Yy1*-KO but was impaired in *Sfpq*-KO mice, and muscle mass and body weight in *Yy1*-KO mice are normal until 2 months of age (Blattler et al., 2012). This implies that

diminished oxidative capacity can be compensated by glycogenolysis to meet energy requirements, resulting in milder phenotypes related to muscle mass and body weight in *Yy1*-KO as compared with *Sfpq*-KO mice. This is supported by a previous report that double knockout of *PGC1α*/β in skeletal muscle caused dysregulation of mitochondrial biogenesis but was indistinguishable from control mice in normal condition; however, these mice exhibited dramatic reductions in exercise tolerance owing to rapid depletion of muscle glycogen stores (Zechner et al., 2010).

Muscle mass is regulated by the signaling pathway of IGF1-AKT-mTOR (Schiaffino and Mammucari, 2011), and mTOR is a primary metabolic regulator of both glycogen and mitochondrial metabolism, indicating that maintenance of muscle mass is closely related to metabolism regulation. Mice with skeletal-muscle-specific *mTOR*-KO showed glycogen accumulation and impaired mitochondrial OXPHOS, which was accompanied by reduced muscle mass and body weight and premature death (Risson et al., 2009). Observed phenotypes in *Sfpq*-KO mice well overlapped with those in *mTOR*-KO mice, and these were much severe than those in *Actn3*-, *Yy1*-, and *Pgc1α*/β-KO mice. In *Pgc1α*/β- and *Actn3*-KO mice, either glycogenolysis or mitochondrial metabolism is increased, indicating that these metabolic pathways can mutually compensate each other and that disruption of both can potentially lead to more severe phenotypes as observed in *Sfpq*- or *mTOR*-KO mice. Additionally, patients with metabolic myopathies such as mitochondrial myopathies and glycogen storage diseases often present with growth failure (Blattler et al., 2012; Slonim et al., 1984; Wolny et al., 2009). These findings support our conjecture that dysregulated energy metabolism in skeletal muscle is an underlying cause of impaired postnatal skeletal muscle development and whole-body growth.

Loss of *Sfpq* downregulated genes the lengths of which are not extra-long. We had found that SFPQ co-transcriptionally activates the transcriptional elongation of pre-mRNAs possessing relatively longer introns (Takeuchi et al., 2018) and affects the expression of genes <100 kbp. Moreover, SFPQ has multifunction such as mRNA processing, transcriptional regulation, and DNA repair (Dong et al., 2007; Ha et al., 2011; Kaneko et al., 2007; Patton et al., 1993; Yarosh et al., 2015). It is possible that loss of *Sfpq* disrupted shorter gene expression and mRNA regulation and subsequently affected the phenotype. As we are analyzing the binding rules of SFPQ to pre-mRNAs and relationship between SFPQ bindings and mRNA regulations, further studies would decipher the roles of SFPQ more precisely in muscle energy metabolism.

SFPQ has been implicated in various diseases including familial amyotrophic lateral sclerosis (ALS) (Thomas-Jinu et al., 2017), frontotemporal lobar degeneration (Ishigaki et al., 2017), and autism spectrum disorder (Chang et al., 2015; O'Roak et al., 2012). About 40% of myopathies have yet to be genetically characterized (Risson et al., 2009). The disease-causing mechanism and pathogenesis of aging-related diseases are still largely unknown. Mitochondrial dysfunction is a cornerstone of aging and loss of muscle mass (Dirks et al., 2006; Konopka and Sreekumaran Nair, 2013). Thus, mutations in *SFPQ* or dysregulation of SFPQ-dependent energy metabolism could underlie idiopathic myopathies or sarcopenia (Risson et al., 2009; Thomas-Jinu et al., 2017). It remains unclear whether exercise tolerance and metabolic changes are reduced in KO mice, whether SFPQ actively regulates energy production in skeletal muscle, and whether therapeutic strategies targeting SFPQ are a viable treatment for metabolic myopathies that should be addressed with further studies. The finding of metabolic pathway gene expression maintained by SFPQ provides an insight into the synergistic network of energy metabolism by RBP with signal transduction and transcriptional regulations in skeletal muscle associating with muscle growth and maintenance and also pathogenesis of muscular dystrophies or metabolic myopathies.

Limitations of the Study

We demonstrated that loss of *Sfpq* in skeletal muscle caused long-gene transcriptopathy and downregulated metabolic pathway-relating genes. RBPs regulate broader genes and add variety and complexity. Thus, it is expected that RBPs plays multiple and essential roles; however, analyses of RBPs tend to be difficult to simply show their functions. We observed severe muscle mass reduction in KO mice but could not eliminate the possibility that effects other than long-gene transcriptopathy affect the observed phenotype. We are challenging to decipher the relationship between binding rules, target specificities, and functions of RBPs that would overcome these technical limits in the near future. In addition, loss of *Sfpq* caused premature death in KO mice with unknown reasons. Severe growth defect with reduced muscle mass, kyphosis, and dysregulation of systemic metabolism affect each other and might contribute to the observed phenotypes. Further study using a different Cre-line may help understand the cause of death and the network regulating muscle mass, muscle energy metabolism, and systemic homeostasis.

METHODS

All methods can be found in the accompanying Transparent Methods supplemental file.

SUPPLEMENTAL INFORMATION

Supplemental Information can be found online at https://doi.org/10.1016/j.isci.2019.02.023.

ACKNOWLEDGMENTS

We thank the Medical Research Support Center for performing high-throughput sequencing analysis and mouse behavioral tests and the Institute of Laboratory Animals, Graduate School of Medicine, Kyoto University, for providing animal care; Dr. Steven J. Burden of Skirball Institute for Molecular Medicine for providing *Mlc1f-Cre* transgenic mice; Dr. Satoru Noguchi and Dr. Miho Miyakawa of Department of Neuromuscular Research, National Institute of Neurosciences, National Center of Neurology and Psychiatry (NCNP) for technical advice in histological analysis; A. Hagiwara, K. Wanezaki, and Y. Takahashi for technical assistance; Dr. T. Tsubota, Dr. Y. Okuno, M. Denawa, Y. Sako, Y. Qi, and members of the M.H. laboratory at Kyoto University for their helpful comments and technical advice; and Editage (www.editage.jp) for English language editing. This work was supported in part by Grants-in-Aid for Scientific Research from the Ministry of Education, Culture, Sports, Science and Technology of Japan (MEXT; Japan Society for the Promotion of Science KAKENHI 19500269, 25500288, 21249013, 15H05721) (to M. Hagaiwara and A.T.); Innovative Cell Biology by Innovating Technology (Cell Innovation) (to M. Hagaiwara, K.O., and A.T.); a Core Research for Evolutional Science and Technology grant from the Japan Science and Technology Agency (to M. Hagaiwara); Intramural Research Grant 25-5 and 28-6 for Neurological and Psychiatric Disorders of NCNP (to M. Hagaiwara); a grant from the Japan Agency for Medical Research and Development (AMED) (to M. Hagaiwara); Platform for Dynamic Approaches to Living System from the MEXT and AMED (to M.H.); iCeMS Cross-Disciplinary Research Promotion Project of Kyoto University (to A.T.); and the Fujiwara Memorial Foundation (to A.T.).

AUTHOR CONTRIBUTIONS

M. Hosokawa conducted most of the experiments, contributed to data analysis, and wrote the manuscript. A.T. conceived and designed the project, conducted animal experiments including the mouse survival assay, supervised all experiments, and prepared the manuscript. J.T. and S.T. provided technical supervision and assisted with muscle phenotype analyses in animal experiments. K.I. analyzed the high-throughput sequencing data. M. Hagiwara conceived the project and prepared the manuscript. All authors contributed to manuscript preparation.

DECLARATION OF INTERESTS

The authors declare no conflicts of interest.

Received: August 24, 2018
Revised: December 27, 2018
Accepted: February 22, 2019
Published: March 29, 2019

REFERENCES

Beauchamp, N.J., Dalton, A., Ramaswami, U., Niinikoski, H., Mention, K., Kenny, P., Kolho, K.L., Raiman, J., Walter, J., Treacy, E., et al. (2007). Glycogen storage disease type IX: high variability in clinical phenotype. Mol. Genet. Metab. *92*, 88–99.

Blattler, S.M., Verdeguer, F., Liesa, M., Cunningham, J.T., Vogel, R.O., Chim, H., Liu, H., Romanino, K., Shirihai, O.S., Vazquez, F., et al. (2012). Defective mitochondrial morphology and bioenergetic function in mice lacking the transcription factor Yin Yang 1 in skeletal muscle. Mol. Cell. Biol. *32*, 3333–3346.

Bothe, G.W., Haspel, J.A., Smith, C.L., Wiener, H.H., and Burden, S.J. (2000). Selective expression of Cre recombinase in skeletal muscle fibers. Genesis *26*, 165–166.

Brocca, L., Cannavino, J., Coletto, L., Biolo, G., Sandri, M., Bottinelli, R., and Pellegrino, M.A. (2012). The time course of the adaptations of human muscle proteome to bed rest and the underlying mechanisms. J. Physiol. *590*, 5211–5230.

Burwinkel, B., Maichele, A.J., Aagenaes, O., Bakker, H.D., Lerner, A., Shin, Y.S., Strachan, J.A., and Kilimann, M.W. (1997). Autosomal glycogenosis of liver and muscle due to phosphorylase kinase deficiency is caused by mutations in the phosphorylase kinase beta subunit (PHKB). Hum. Mol. Genet. *6*, 1109–1115.

Carmignac, V., Svensson, M., Korner, Z., Elowsson, L., Matsumura, C., Gawlik, K.I., Allamand, V., and Durbeej, M. (2011). Autophagy is increased in laminin alpha2 chain-deficient muscle and its inhibition improves muscle morphology in a mouse model of MDC1A. Hum. Mol. Genet. *20*, 4891–4902.

Carson, J.A., Hardee, J.P., and VanderVeen, B.N. (2016). The emerging role of skeletal muscle oxidative metabolism as a biological target and cellular regulator of cancer-induced muscle wasting. Semin. Cell Dev. Biol. *54*, 53–67.

Chang, J., Gilman, S.R., Chiang, A.H., Sanders, S.J., and Vitkup, D. (2015). Genotype to

phenotype relationships in autism spectrum disorders. Nat. Neurosci. *18*, 191–198.

Connolly, A.M., Keeling, R.M., Mehta, S., Pestronk, A., and Sanes, J.R. (2001). Three mouse models of muscular dystrophy: the natural history of strength and fatigue in dystrophin-, dystrophin/utrophin-, and laminin alpha2-deficient mice. Neuromuscul. Disord. *11*, 703–712.

Cortese, A., Plagnol, V., Brady, S., Simone, R., Lashley, T., Acevedo-Arozena, A., de Silva, R., Greensmith, L., Holton, J., Hanna, M.G., et al. (2014). Widespread RNA metabolism impairment in sporadic inclusion body myositis TDP43-proteinopathy. Neurobiol. Aging *35*, 1491–1498.

Cosker, K.E., Fenstermacher, S.J., Pazyra-Murphy, M.F., Elliott, H.L., and Segal, R.A. (2016). The RNA-binding protein SFPQ orchestrates an RNA regulon to promote axon viability. Nat. Neurosci. *19*, 690–696.

Cunningham, J.T., Rodgers, J.T., Arlow, D.H., Vazquez, F., Mootha, V.K., and Puigserver, P. (2007). mTOR controls mitochondrial oxidative function through a YY1-PGC-1alpha transcriptional complex. Nature *450*, 736–740.

Dirks, A.J., Hofer, T., Marzetti, E., Pahor, M., and Leeuwenburgh, C. (2006). Mitochondrial DNA mutations, energy metabolism and apoptosis in aging muscle. Ageing Res. Rev. *5*, 179–195.

Dong, X., Sweet, J., Challis, J.R., Brown, T., and Lye, S.J. (2007). Transcriptional activity of androgen receptor is modulated by two RNA splicing factors, PSF and p54nrb. Mol. Cell. Biol. *27*, 4863–4875.

Gabel, H.W., Kinde, B., Stroud, H., Gilbert, C.S., Harmin, D.A., Kastan, N.R., Hemberg, M., Ebert, D.H., and Greenberg, M.E. (2015). Disruption of DNA-methylation-dependent long gene repression in Rett syndrome. Nature *522*, 89–93.

Gan, Z., Rumsey, J., Hazen, B.C., Lai, L., Leone, T.C., Vega, R.B., Xie, H., Conley, K.E., Auwerx, J., Smith, S.R., et al. (2013). Nuclear receptor/microRNA circuitry links muscle fiber type to energy metabolism. J. Clin. Invest. *123*, 2564–2575.

Goodman, C.A., Mabrey, D.M., Frey, J.W., Miu, M.H., Schmidt, E.K., Pierre, P., and Hornberger, T.A. (2011). Novel insights into the regulation of skeletal muscle protein synthesis as revealed by a new nonradioactive in vivo technique. FASEB J. *25*, 1028–1039.

Gudiksen, A., and Pilegaard, H. (2017). PGC-1alpha and fasting-induced PDH regulation in mouse skeletal muscle. Physiol. Rep. *5*, e13222.

Ha, K., Takeda, Y., and Dynan, W.S. (2011). Sequences in PSF/SFPQ mediate radioresistance and recruitment of PSF/SFPQ-containing complexes to DNA damage sites in human cells. DNA Repair (Amst.) *10*, 252–259.

Ishigaki, S., Fujioka, Y., Okada, Y., Riku, Y., Udagawa, T., Honda, D., Yokoi, S., Endo, K., Ikenaka, K., Takagi, S., et al. (2017). Altered Tau Isoform ratio caused by loss of FUS and SFPQ function leads to FTLD-like phenotypes. Cell Rep. *18*, 1118–1131.

Kanehisa, M., and Goto, S. (2000). KEGG: kyoto encyclopedia of genes and genomes. Nucleic Acids Res. *28*, 27–30.

Kaneko, S., Rozenblatt-Rosen, O., Meyerson, M., and Manley, J.L. (2007). The multifunctional protein p54nrb/PSF recruits the exonuclease XRN2 to facilitate pre-mRNA 3' processing and transcription termination. Genes Dev. *21*, 1779–1789.

Keene, J.D. (2007). RNA regulons: coordination of post-transcriptional events. Nat. Rev. Genet. *8*, 533–543.

King, I.F., Yandava, C.N., Mabb, A.M., Hsiao, J.S., Huang, H.S., Pearson, B.L., Calabrese, J.M., Starmer, J., Parker, J.S., Magnuson, T., et al. (2013). Topoisomerases facilitate transcription of long genes linked to autism. Nature *501*, 58–62.

Konopka, A.R., and Sreekumaran Nair, K. (2013). Mitochondrial and skeletal muscle health with advancing age. Mol. Cell. Endocrinol. *379*, 19–29.

Lagier-Tourenne, C., Polymenidou, M., Hutt, K.R., Vu, A.Q., Baughn, M., Huelga, S.C., Clutario, K.M., Ling, S.C., Liang, T.Y., Mazur, C., et al. (2012). Divergent roles of ALS-linked proteins FUS/TLS and TDP-43 intersect in processing long pre-mRNAs. Nat. Neurosci. *15*, 1488–1497.

Laplante, M., and Sabatini, D.M. (2012). mTOR signaling in growth control and disease. Cell *149*, 274–293.

MacArthur, D.G., Seto, J.T., Chan, S., Quinlan, K.G., Raftery, J.M., Turner, N., Nicholson, M.D., Kee, A.J., Hardeman, E.C., Gunning, P.W., et al. (2008). An Actn3 knockout mouse provides mechanistic insights into the association between alpha-actinin-3 deficiency and human athletic performance. Hum. Mol. Genet. *17*, 1076–1086.

Matthews, L., Gopinath, G., Gillespie, M., Caudy, M., Croft, D., de Bono, B., Garapati, P., Hemish, J., Hermjakob, H., Jassal, B., et al. (2009). Reactome knowledgebase of human biological pathways and processes. Nucleic Acids Res. *37*, D619–D622.

Mouisel, E., Relizani, K., Mille-Hamard, L., Denis, R., Hourde, C., Agbulut, O., Patel, K., Arandel, L., Morales-Gonzalez, S., Vignaud, A., et al. (2014). Myostatin is a key mediator between energy metabolism and endurance capacity of skeletal muscle. Am. J. Physiol. Regul. Integr. Comp. Physiol. *307*, R444–R454.

Mourkioti, F., Slonimsky, E., Huth, M., Berno, V., and Rosenthal, N. (2008). Analysis of CRE-mediated recombination driven by myosin light chain 1/3 regulatory elements in embryonic and adult skeletal muscle: a tool to study fiber specification. Genesis *46*, 424–430.

O'Roak, B.J., Vives, L., Girirajan, S., Karakoc, E., Krumm, N., Coe, B.P., Levy, R., Ko, A., Lee, C., Smith, J.D., et al. (2012). Sporadic autism exomes reveal a highly interconnected protein network of de novo mutations. Nature *485*, 246–250.

Oh, J.M., Di, C., Venters, C.C., Guo, J., Arai, C., So, B.R., Pinto, A.M., Zhang, Z., Wan, L., Younis, I., et al. (2017). U1 snRNP telescripting regulates a size-function-stratified human genome. Nat. Struct. Mol. Biol. *24*, 993–999.

Patel, S., Doble, B.W., MacAulay, K., Sinclair, E.M., Drucker, D.J., and Woodgett, J.R. (2008). Tissue-specific role of glycogen synthase kinase 3beta in glucose homeostasis and insulin action. Mol. Cell. Biol. *28*, 6314–6328.

Patton, J.G., Porro, E.B., Galceran, J., Tempst, P., and Nadal-Ginard, B. (1993). Cloning and characterization of PSF, a novel pre-mRNA splicing factor. Genes Dev. *7*, 393–406.

Polymenidou, M., Lagier-Tourenne, C., Hutt, K.R., Huelga, S.C., Moran, J., Liang, T.Y., Ling, S.C., Sun, E., Wancewicz, E., Mazur, C., et al. (2011). Long pre-mRNA depletion and RNA missplicing contribute to neuronal vulnerability from loss of TDP-43. Nat. Neurosci. *14*, 459–468.

Quinlan, K.G., Seto, J.T., Turner, N., Vandebrouck, A., Floetenmeyer, M., Macarthur, D.G., Raftery, J.M., Lek, M., Yang, N., Parton, R.G., et al. (2010). Alpha-actinin-3 deficiency results in reduced glycogen phosphorylase activity and altered calcium handling in skeletal muscle. Hum. Mol. Genet. *19*, 1335–1346.

Risson, V., Mazelin, L., Roceri, M., Sanchez, H., Moncollin, V., Corneloup, C., Richard-Bulteau, H., Vignaud, A., Baas, D., Defour, A., et al. (2009). Muscle inactivation of mTOR causes metabolic and dystrophin defects leading to severe myopathy. J. Cell Biol. *187*, 859–874.

Rogelj, B., Easton, L.E., Bogu, G.K., Stanton, L.W., Rot, G., Curk, T., Zupan, B., Sugimoto, Y., Modic, M., Haberman, N., et al. (2012). Widespread binding of FUS along nascent RNA regulates alternative splicing in the brain. Sci. Rep. *2*, 603.

Savarese, M., Sarparanta, J., Vihola, A., Udd, B., and Hackman, P. (2016). Increasing role of titin mutations in neuromuscular disorders. J. Neuromuscul. Dis. *3*, 293–308.

Schiaffino, S., and Mammucari, C. (2011). Regulation of skeletal muscle growth by the IGF1-Akt/PKB pathway: insights from genetic models. Skelet. Muscle *1*, 4.

Schiaffino, S., and Reggiani, C. (1994). Myosin isoforms in mammalian skeletal muscle. J. Appl. Physiol. (1985) *77*, 493–501.

Singh, R.K., Kolonin, A.M., Fiorotto, M.L., and Cooper, T.A. (2018). Rbfox-splicing factors maintain skeletal muscle mass by regulating calpain3 and proteostasis. Cell Rep. *24*, 197–208.

Slonim, A.E., Coleman, R.A., and Moses, W.S. (1984). Myopathy and growth failure in debrancher enzyme deficiency: improvement with high-protein nocturnal enteral therapy. J. Pediatr. *105*, 906–911.

Stefanetti, R.J., Lamon, S., Wallace, M., Vendelbo, M.H., Russell, A.P., and Vissing, K. (2015). Regulation of ubiquitin proteasome pathway molecular markers in response to endurance and resistance exercise and training. Pflugers Arch. *467*, 1523–1537.

Subramanian, A., Tamayo, P., Mootha, V.K., Mukherjee, S., Ebert, B.L., Gillette, M.A., Paulovich, A., Pomeroy, S.L., Golub, T.R., Lander, E.S., et al. (2005). Gene set enrichment analysis: a knowledge-based approach for interpreting

genome-wide expression profiles. Proc. Natl. Acad. Sci. U S A *102*, 15545–15550.

Sugino, K., Hempel, C.M., Okaty, B.W., Arnson, H.A., Kato, S., Dani, V.S., and Nelson, S.B. (2014). Cell-type-specific repression by methyl-CpG-binding protein 2 is biased toward long genes. J. Neurosci. *34*, 12877–12883.

Takeuchi, A., Iida, K., Tsubota, T., Hosokawa, M., Denawa, M., Brown, J.B., Ninomiya, K., Ito, M., Kimura, H., Abe, T., et al. (2018). Loss of Sfpq causes long-gene transcriptopathy in the brain. Cell Rep. *23*, 1326–1341.

Thomas-Jinu, S., Gordon, P.M., Fielding, T., Taylor, R., Smith, B.N., Snowden, V., Blanc, E., Vance, C., Topp, S., Wong, C.H., et al. (2017). Non-nuclear pool of splicing factor SFPQ regulates axonal transcripts required for normal motor development. Neuron *94*, 322–336.e5.

Tipton, K.D., Hamilton, D.L., and Gallagher, I.J. (2018). Assessing the role of muscle protein breakdown in response to nutrition and exercise in humans. Sports Med. *48* (*Suppl 1*), 53–64.

Vainzof, M., Ayub-Guerrieri, D., Onofre, P.C., Martins, P.C., Lopes, V.F., Zilberztajn, D., Maia, L.S., Sell, K., and Yamamoto, L.U. (2008). Animal models for genetic neuromuscular diseases. J. Mol. Neurosci. *34*, 241–248.

van Putten, M., Hulsker, M., Nadarajah, V.D., van Heiningen, S.H., van Huizen, E., van Iterson, M., Admiraal, P., Messemaker, T., den Dunnen, J.T., t Hoen, P.A., et al. (2012). The effects of low levels of dystrophin on mouse muscle function and pathology. PLoS One *7*, e31937.

Wolny, S., McFarland, R., Chinnery, P., and Cheetham, T. (2009). Abnormal growth in mitochondrial disease. Acta Paediatr. *98*, 553–554.

Yamamoto, J., Kamata, S., Miura, A., Nagata, T., Kainuma, R., and Ishii, I. (2015). Differential adaptive responses to 1- or 2-day fasting in various mouse tissues revealed by quantitative PCR analysis. FEBS Open Bio. *5*, 357–368.

Yarosh, C.A., Iacona, J.R., Lutz, C.S., and Lynch, K.W. (2015). PSF: nuclear busy-body or nuclear facilitator? Wiley Interdiscip. Rev. RNA *6*, 351–367.

Zechner, C., Lai, L., Zechner, J.F., Geng, T., Yan, Z., Rumsey, J.W., Collia, D., Chen, Z., Wozniak, D.F., Leone, T.C., et al. (2010). Total skeletal muscle PGC-1 deficiency uncouples mitochondrial derangements from fiber type determination and insulin sensitivity. Cell Metab. *12*, 633–642.

Zierath, J.R., and Hawley, J.A. (2004). Skeletal muscle fiber type: influence on contractile and metabolic properties. PLoS Biol. *2*, e348.

ISCI, Volume *13*

Supplemental Information

Loss of RNA-Binding Protein *Sfpq* Causes Long-Gene Transcriptopathy in Skeletal Muscle and Severe Muscle Mass Reduction with Metabolic Myopathy

Motoyasu Hosokawa, Akihide Takeuchi, Jun Tanihata, Kei Iida, Shin'ichi Takeda, and Masatoshi Hagiwara

Supplemental Figures and Legends

Figure S1

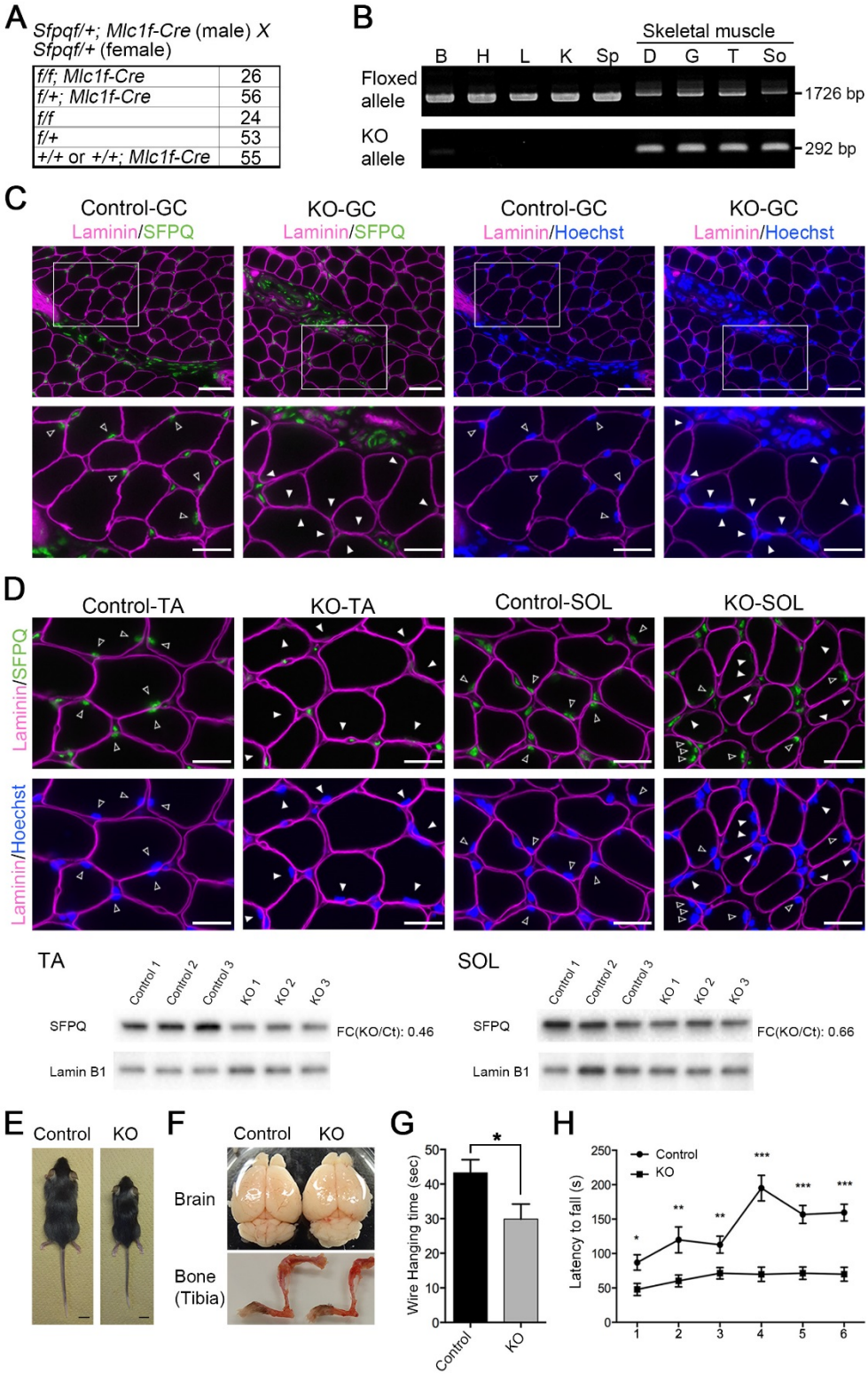

Figure S1. Phenotypic analysis of *Sfpq* KO mice, related to Figure 1. (A) Offspring ratio of male *Sfpq* conditional knockout mice obtained by crossing *Sfpq*$^{f/+}$*;Mlc1f-Cre* male mice with *Sfpq*$^{f/+}$ female mice (from P7 to P14). *f*, floxed; +, wild type. **(B)** Examination of Cre excision in several tissues from *KO* mice. Genotyping polymerase chain reaction (PCR) was performed to detect the floxed (Floxed allele; 1726 bp) and *Sfpq* knockout alleles after Cre excision [KO allele; 292 bp]. B, brain; D, diaphragm; G, gastrocnemius; H, heart; K, kidney; L, liver; Sp, spleen; T, tibialis anterior; So, soleus (female). **(C, D)** Immunostaining for SFPQ (green) and Laminin (purple) nuclear counterstained with Hoechst 33342 on gastrocnemius muscles (GC) (C), tibialis anterior (TA) and soleus muscles (SOL) (D, upper panel) from 1-month-old male KO and control mice. Scale bars: 50 μm. Boxed areas indicated in upper panels are shown with higher magnification in lower panels. Scale bar = 25 μm. Open arrow heads indicate nuclei in myofiber which are positively stained with SFPQ antibody and closed white arrow heads indicate nuclei which are negative for SFPQ. Western Blotting (WB) for SFPQ protein expression in TA and SOL muscle samples from 1-month-old male KO and control mice (n = 3 in each genotype). Lamin B1 was used as control for the equal sample loading. Averaged fold changes (FCs) between *Sfpq*-KO and control (KO/Ct) mice were indicated (D, lower panel). **(E)** Gross appearance of male KO and control mice at P35. Scale bars: 10 mm. **(F)** Representative photos of brain and bone (tibia) from 1-month-old male KO and control mice. **(G)** Wire hang test performed on male KO (n = 19) and control (n = 20) mice from P26 to P30. The test lasted 60 s. Data are presented as mean ± SEM. *$p < 0.05$ (Student's t test) **(H)** Rotarod test performed on male KO (n = 15) and control (n = 20) mice from P26 to P30. Data are presented as mean ± SEM. *$p < 0.05$, **$p < 0.01$, ***$p < 0.001$ versus control (Student's t test or Welch's t test).

Figure S2

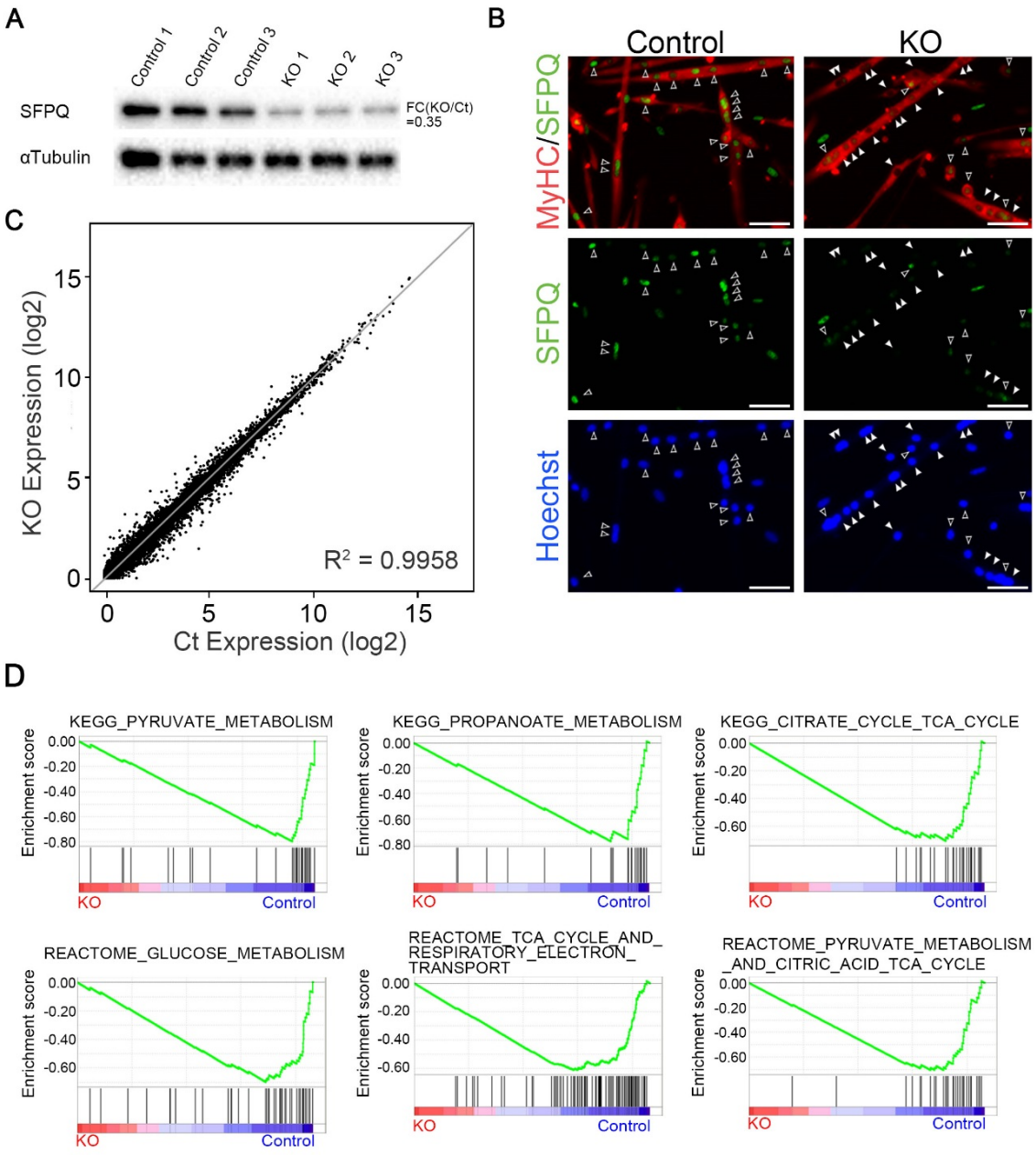

E

Gene	Disease
Phkb (*phosphorylase kinase beta*)	Glycogen storage disease IXb
Gbel [*glucan (1,4-alpha-), branching enzyme 1*]	Glycogen storage disease IV
Pcx (*pyruvate carboxylase*)	Pyruvate carboxylase deficiency
Hlcs (*holocarboxylase synthetase*)	Multiple carboxylase deficiency
Pcca (*propionyl-Coenzyme A carboxylase, alpha polypeptide*)	Propionic acidaemia
Suclg2 (*succinate-Coenzyme A ligase, GDP-forming, beta subunit*)	Methylmalonic aciduria
Lpin1 (*lipin 1*)	Myoglobinuria recurrent

Figure S2. Transcriptome analysis and GSEA on *Sfpq* KO myotubes, related to Figure 3 and 4. (A) WB showing SFPQ protein expression in KO and control myotubes which were induced differentiation for 4 days. α-Tubulin was used as the control for equal sample loading. Averaged FC between *Sfpq*-KO and control (KO/Ct) myotubes was indicated. **(B)** Immunostaining for SFPQ (green) and MyHC (red) nuclear counterstained with Hoechst 33342 on KO and control myotubes which were induced differentiation for 4 days. Open arrow heads indicate nuclei in MyHC-positive differentiated myotubes which are positively stained with SFPQ antibody and closed white arrow heads indicate nuclei which are negative for SFPQ. Scale bars: 50 μm. **(C)** Scatterplot showing mRNA expression in KO (n = 3) and control myotubes (n = 3) determined by polyA-selected mRNA-seq. X- and y-axes show $\log_2$ of average mRNA expression in three control and three KO myotubes, respectively. Ct, control; KO, knockout; R^2, coefficient of determination. **(D)** Representative GSEA plot of the gene sets in Figure 3C and 3D. **(E)** Downregulated genes in KO myotubes and their association with inherited metabolic diseases. SFPQ target genes, which showed 3´-site downregulation, were shown with red characters.

Figure S3

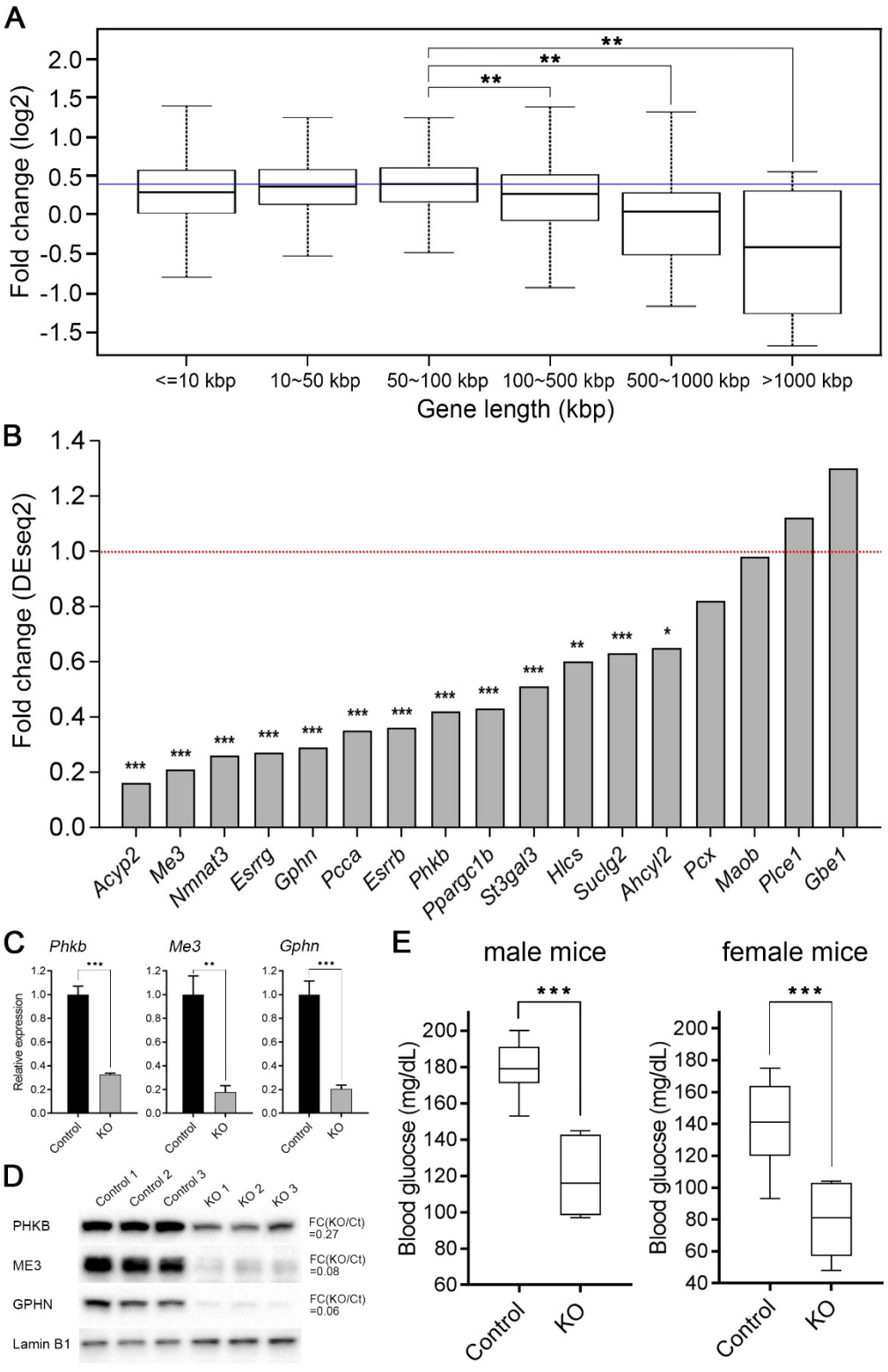
A
Fold change (log2)
2.0
1.5
1.0
0.5
0.0
-0.5
-1.0
-1.5
**
**
**
<=10 kbp
10~50 kbp
50~100 kbp
100~500 kbp
500~1000 kbp
>1000 kbp
Gene length (kbp)
B
Fold change (DEseq2)
1.4
1.2
1.0
0.8
0.6
0.4
0.2
0.0
Acyp2
Me3
Nmnat3
Esrrg
Gphn
Pcca
Esrrb
Phkb
Ppargc1b
St3gal3
Hlcs
Suclg2
Ahcyl2
Pcx
Maob
Plce1
Gbe1
C
Phkb
Me3
Gphn
Relative expression
Control
KO
D
Control 1
Control 2
Control 3
KO 1
KO 2
KO 3
PHKB
ME3
GPHN
Lamin B1
FC(KO/Ct) =0.27
FC(KO/Ct) =0.08
FC(KO/Ct) =0.06
E
male mice
female mice
Blood glucose (mg/dL)
Control
KO

Figure S3. *In vivo* transcriptome analysis in *Sfpq* KO mice and blood glucose measurement related to Figure 3 and 4. (A) Box plots showing length-dependent gene expression changes in KO-GC muscle from P35 male mice (n = 3). Bins were defined according to gene length. $^{**}p < 0.001$ for changes between two bins (Mann-Whitney U test). The baseline was drawn at the mean value in 50-100 kbp genes (fold change = 0.40). **(B)** The fold changes of mRNA levels in KO muscles for all downregulated genes > 100 kbp in GSEA identified metabolic pathway genes and transcriptional regulators in KO myotubes. Fold changes and q values were calculated using DESeq2 for analyzing RNA-seq data of GC muscle samples from P35 male KO and control mice (n = 3). $^{*}q < 0.05$, $^{**}q < 0.001$ and $^{***}q < 0.001$. **(C)** RT-qPCR quantification of indicated genes in GC muscle samples from P35 male KO and control mice (n = 3). Data are presented as mean ± SD. $^{**}p < 0.01$, $^{***}p < 0.001$ (Student's t test). **(D)** WB for PHKB, ME3 and GPHN proteins on TA muscles from 1-month-old male KO and control mice (n = 3). Lamin B1 was used as control for the equal sample loading. Averaged FCs between *Sfpq* KO and control (Ct) mice (KO/Ct) were indicated. **(E)** Blood glucose concentrations were measured in 4-5-week-old male (*left*) and female (*right*) KO and control mice after 6-hour fast. (male: n = 6, female: n = 7). $^{***}p < 0.001$ (Student's t test)

Figure S4

A Protein degradation markers

	Gene symbol	FC(KO/Ct)	*q* value
Ubiqitin-Proteasome	*Fbxo32* (*F-box protein 32*) (*Atrogin1*)	1.17	0.76
	Trim63 (*tripartite motif-containing 63*)(*Murf1*)	1.08	0.72
	Foxo1 (*forkhead box O1*)	1.00	1.00
	Foxo3 (*forkhead box O3*)	1.13	0.60
	Fbxo40 (*F-box protein 40*)	0.91	0.52
Calpain-Calpastatin	*Capn1* (*calpain 1*)	1.21	0.07
	Capn2 (*calpain 2*)	1.22	0.08
	Capn3 (*calpain 3*)	0.89	0.46
Lysosome-Autophagy	*Map1lc3b* (*microtubule-associated protein 1 light chain 3 beta*) (*LC3b*)	0.98	0.93
	Lamp2 (*lysosomal-associated membrane protein 2*)	0.82	0.32
	Sqstm1 (*sequestosome 1*) (*p62*)	1.18	0.14
	Ctsl (*cathepsin L*)	1.44	0.0004***
	Gabarapl1 (*gamma-aminobutyric acid (GABA) A receptor-associated protein-like 1*)	1.04	0.88
	Atg4b (*autophagy related 4B, cysteine peptidase*)	1.05	0.84
	Atg12 (*autophagy related 12*)	0.83	0.34
	Bnip3 (*BCL2/adenovirus E1B interacting protein 3*)	0.99	0.94
	Bnip3l (*BCL2/adenovirus E1B interacting protein 3-like*)	1.20	0.20
	Becn1 (*beclin 1, autophagy related*)	0.93	0.71

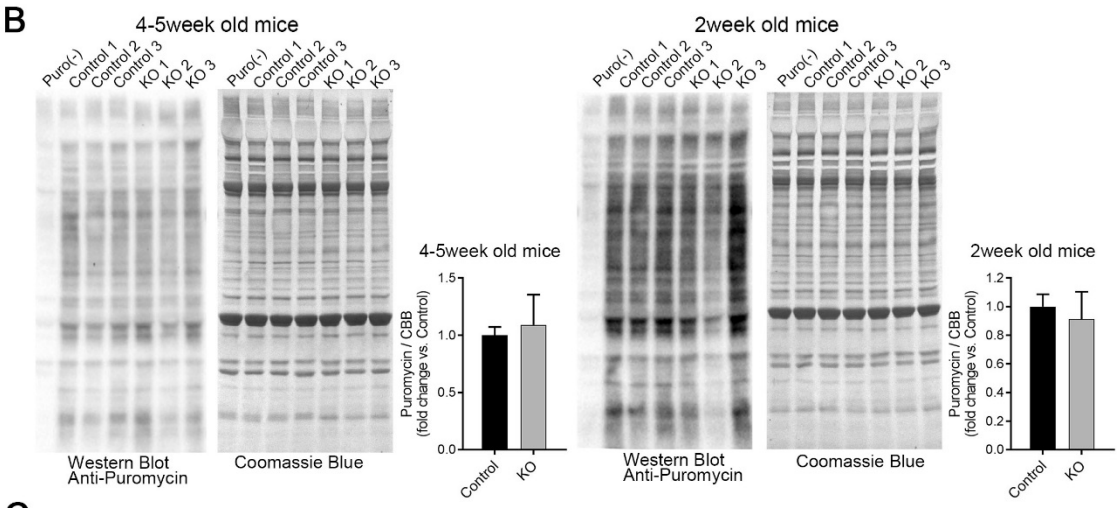

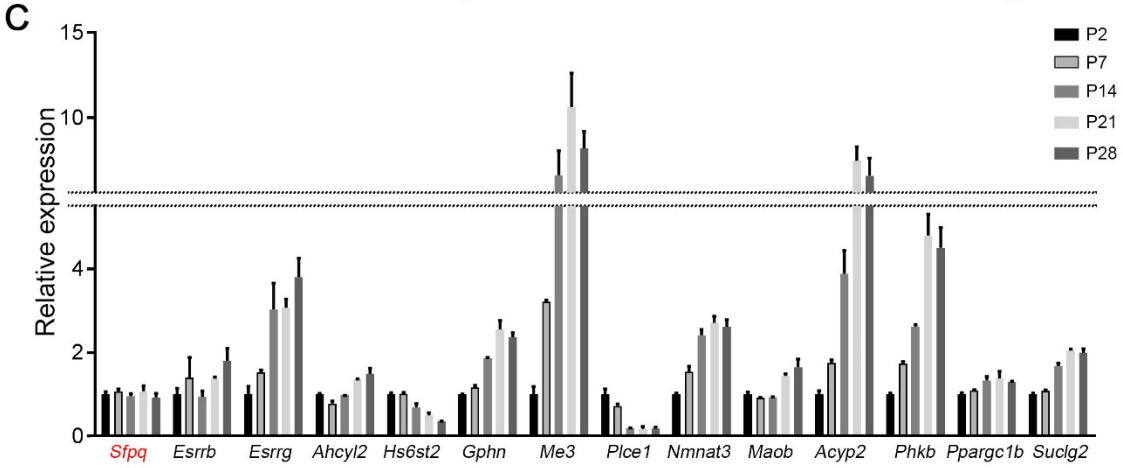

Figure S4. Catabolic and anabolic activities in KO muscle tissues, expression change of SFPQ target genes in during postnatal muscle development, related to Figure 3 and 4. **(A)** FCs and *q* values of genes relating to protein degradation. FCs and *q* values were calculated using DESeq2 for RNA-seq data of GC muscle samples from P35 male KO and control mice ($n = 3$). ***$q < 0.001$. **(B)** WB for Puromycin-labeled newly synthesized protein from 4-5 week (*left*) and 2 week (*right*) old male KO and control mice ($n = 3$). Coomassie Blue staining (CBB) of membranes was conducted to verify equal sample loading. Intensity of total lanes in WB of Puromycin antibody was measured and adjusted by CBB stained signal to measure the total synthesized proteins per loaded proteins, and relative fold changes of synthesized proteins were plotted. Data are presented as mean ± SD. There were no significant differences between KO and Control (Student's t test). **(C)** The mRNA expression levels of *Sfpq* and SFPQ target genes, which showed 3′-site downregulation, in control (wild-type) GC muscle samples collected at indicated developmental stages ($n = 2$). Data was shown as relative mRNA levels of those in postnatal day 2 (P2) for comparison. Data are presented as mean ± SD.

Supplemental Table

Table S1. Genes downregulated in KO myotubes in the GSEA, related to Figure 4.

Gene symbol	Fold change	*p* value	Gene length	Regulatory pathway	*
Genes extracted from downregulated KEGG gene sets					
Gmds	0.52	2E-06	**518959**	Fructose and mannose metabolism	
Gphn	0.54	4E-09	**458118**	Folate biosynthesis	
Pcca	0.69	0.0006	**355617**	Carbon metabolism, etc.	1)
Plce1	0.68	0.0010	**260909**	Inositol phosphate metabolism	
Gbe1	0.59	0.0012	**255772**	Starch and sucrose metabolism	2)
Suclg2	0.72	0.0005	**245838**	Carbon metabolism, etc.	3)
Me3	0.49	5E-09	**221542**	Pyruvate metabolism, etc.	
St3gal3	0.72	0.0014	**202794**	Mannose type O-glycan biosynthesis	
Hlcs	0.69	0.0002	**158551**	Biotin metabolism	4)
Ahcyl2	0.61	6E-07	**143868**	Cysteine and methionine metabolism	
Acyp2	0.55	2E-05	**143405**	Pyruvate metabolism, etc.	
Nmnat3	0.53	1E-05	**114846**	Nicotinate and nicotinamide metabolism	
Pcx	0.71	2E-05	**111281**	Carbon metabolism, etc.	5)
Maob	0.70	0.0008	**108086**	Arginine and proline metabolism, etc.	
Plpp3	0.66	0.0007	75421	Glycerolipid metabolism, etc.	
Lpin1	0.58	0.0004	54102	Glycerolipid metabolism, etc.	6)
Acsl1	0.68	0.0010	45086	Fatty acid metabolism	
Kyat3	0.59	0.0009	43864	Tryptophan catabolism, etc.	
Galnt5	0.59	2E-06	41017	Mucin type O-glycan biosynthesis	
Pon3	0.62	6E-06	35382	Metabolic pathways	
Idh1	0.69	1E-07	27864	2-Oxocarboxylic acid metabolism	
Got1	0.53	2E-06	24854	2-Oxocarboxylic acid metabolism	
Bdh2	0.54	0.0001	23206	Butanoate metabolism	
Oat	0.71	0.0009	18924	Arginine and proline metabolism, etc.	
Extl1	0.55	8E-06	16175	Glycosaminoglycan biosynthesis	
Hmox1	0.67	0.0009	6976	Porphyrin and chlorophyll metabolism	
Cycs	0.75	0.0020	3912	Sulfur metabolism	
Cox7a1	0.59	0.0003	1860	Oxidative phosphorylation	
Genes extracted from downregulated Reactome gene sets (except for above genes)					
Hs6st2	0.62	9E-07	**294966**	Metabolism of carbohydrates	
Phkb	0.69	3E-06	**219641**	Metabolism of carbohydrates, etc.	7)
Slc25a12	0.65	0.0018	93260	Gluconeogenesis, etc.	
D2hgdh	0.76	0.0029	27122	TCA cycle, etc.	

*Inherited metabolic disease identified in Human Gene Mutation Database: 1) propionic acidemia, 2) glycogen storage disease IV, 3) methylmalonic aciduria, 4) multiple carboxylase deficiency, 5) pyruvate carboxylase deficiency, 6) myoglobinuria recurrent, and 7) glycogen storage disease IXb.

Transparent Methods

Mice.

Sfpq-floxed mice (accession no. CDB0981K; http://www2.clst.riken.jp/arg/mutant%20mice%20list.html) were generated as previously described (http://www2.clst.riken.jp/arg/Methods.html) (Takeuchi et al., 2018) and were crossed with *Mlc1f-Cre* mice to generate skeletal muscle-specific knockout mice (Bothe et al., 2000). Genotyping PCR was performed using genomic DNA from a finger as previously described (Takeuchi et al., 2018). Cre-mediated excision of the floxed *Sfpq* DNA segments was determined by PCR amplification of genomic DNA isolated from mouse tissues using primers P763-2 and P766. *Cre* transgenes were detected by PCR using primers P1005 and P720 along with those for the internal control (*interleukin-2*). Genotyping primer positions are shown below. Animal care and experiments were in accordance with the National Institutes of Health Guide for the Care and Use of Laboratory Animals, and all experimental protocols were approved by the Institutional Animal Care and Use Committee of Kyoto University Graduate School of Medicine and RIKEN, Kobe Branch.

Sfpq-recombinant alleles
P763-2: 5'-TTGGTGCTGTCTTCCTAGTCTGCATTTAG-3'
P766: 5'-GTATTCATAACACTGGCATGATGGCTCACACCTATA-3'

Mlc1f-Cre with internal control
P1005:5'-CAAGTGTCACTCTGACAGGTTCTTCTGGAGGAG-3'
P720: 5'-TCCATGAGTGAACGAACCTGGTCGAAATCAG-3'
P715: 5'-CTAGGCCACAGAATTGAAAGATCT-3'
P716: 5'-GTAGGTGGAAATTCTAGCATCATCC-3'

Behavioral tests.

Behavioral tests were performed as previously described (Matsuo et al., 2009; Miyakawa et al., 2001). A grip-strength meter (O'Hara & Co., Tokyo, Japan) was used to measure forelimb grip strength. Mice were lifted by their tails to allow their forepaws to grip a wire grid, and with the bodies of the mice parallel to the surface of the table, the mice were gently and continuously pulled back by their tails until they released the grid. The maximum force applied by the forelimbs to grasp the grid was recorded in Newtons (N). The grip-strength test was performed three times for each mouse, and the highest measured value was used for analytical purposes. During the wire hang test, each mouse was placed on a wire mesh that was then inverted and waved gently in order to force the mouse to grip the wire. The time required for mice to fall was recorded, with a 60-s

cut-off time. For the rotarod test, an accelerating rotarod (UGO Basile Accelerating Rotarod) that accelerated from 4 to 40 rpm over a 5-min period was used. The mice were placed on the rotating drums (3 cm diameter), and the time each mouse was able to maintain its balance on the rod was record. The speed of the rotarod accelerated from 4 to 40 rpm over a 5-min period.

Measurement of blood glucose concentration.

Following 6 hour fast, blood glucose concentration was measured from tail vain using Accu-Chek ST Meter (Roche Diagnostics K.K., Tokyo, Japan).

Measurement of glycogen content.

The glycogen content of muscles was measured by modifications of a previously described procedure (Chan and Exton, 1976; Iwasaki et al., 2012; Quinlan et al., 2010). GC Muscles were removed from the KO and control mice. Then, they were incubated in 200µl 1M KOH per 40mg muscle at 70°C for 1hour. Following digestion 75 µL of saturated Na_2SO_4 and 1.725 mL of ethanol was added on ice (final volume 2 mL). Samples were precipitated by centrifuging at 13000 rpm for 10 mins at 4°C. The supernatant was removed and the pellet dissolved in 200 µL dH_2O. Samples were reprecipitated with 1.8 mL ethanol. The supernatant was removed and pellet was dried. The pellets were resuspended in 400 µL Glycogen Hydrolysis Buffer (Abcam, Cambridge, UK). The amount of glycogen was determined with Glycogen Assay Kit (Abcam).

Surface sensing of translation (SUnSET).

For all *in vivo* measurements of protein synthesis with SUnSET (Goodman et al., 2011), puromycin (Merck Millipore, Billerica, MA, USA) stock solution (75mM) was prepared and diluted to the appropriate volume, which was needed to inject mice with 0.04 µmol/g body weight in 200 µl of phosphate-buffered saline (PBS), and subsequently administered into the animals via intraperitoneal injection. At exactly 30 min after injection, muscle tissues were extracted and either frozen in liquid nitrogen for WB analysis as detailed below. After capturing the appropriate image, the membranes were stained with Coomassie Blue (Nacalai Tesque, Kyoto, Japan) to verify equal loading in all lanes. Densitometric measurements were performed by the density of each total lane volume.

H&E staining.

After mice were sacrificed, skeletal muscles were isolated, embedded in tragacanth gum (Wako Pure Chemical Industries, Osaka, Japan), and flash frozen in isopentane cooled in liquid nitrogen. Cryosections (7 µm) of skeletal muscle tissue were stained with H&E as previously described (Tanihata et al., 2008).

Modified Gomori trichrome staining.

Cryosections (10 μm) from skeletal muscle tissue were stained in Gomori solution followed by Harris Hematoxylin (Muto Pure Chemicals, Tokyo, Japan). Gomori solution consists of fast green FCF (Kanto Chemical, Tokyo, Japan), chromotrope 2R (Sigma-Aldrich, St. Louis, MO, USA), phosphotungstic acid (Kanto Chemical) and acetic anhydride (Malicdan et al., 2009).

NADH-TR staining.

Cryosections (10 μm) from skeletal muscle tissue were incubated with NADH-TR staining solution [0.8 mg/ml β-NADH (Sigma-Aldrich) and 1 mg/ml nitro blue tetrazolium (Sigma-Aldrich) in 50 mM Tris–HCl (pH 7.4)] at 37°C. After staining, sections were washed with acetone solution followed by deionized water, and mounted with Glycerol Gelatin (Sigma-Aldrich).

Periodic acid Schiff staining.

Cryosections (10 μm) from skeletal muscle tissue were fixed with Carnoy's fixative (60% methanol, 30% chloroform, and 10% acetic acid) and incubated for 10 min in periodic acid solution (Sigma-Aldrich). Sections were incubated in Schiff's reagent (Sigma-Aldrich) for 10 min and dehydrated.

Immunohistochemistry.

Cryosections (7 μm) obtained from the middle portion of frozen muscles were dried and fixed with 4% paraformaldehyde for SFPQ at room temperature (RT) and acetone for 10 min at −20°C for other 1st antibodies, and pre-incubated in PBS containing 10% goat serum and 0.5% Triton X-100 for 15 min at RT. Primary antibodies were applied overnight at 4°C with 15% goat serum followed by 30 min at RT with secondary antibodies. The antibodies used were raised polyclonal for SFPQ (1:800) (Takeuchi et al., 2018), mouse monoclonal anti-MyHC type I [1:100; BA-D5-c, the Developmental Studies Hybridoma Bank maintained by the University of Iowa (DSHB), Iowa City, IA, USA], mouse monoclonal anti-MyHC type IIA (1:200; SC-71-c, DSHB), mouse monoclonal anti-MyHC type IIB (1:200; BF-F3-c, DSHB) and rat monoclonal laminin 2 (1:200; 4H8-2: Cat#ALX-804-190-C100, Enzo Life Sciences, Farmingdale, NY, USA), followed by Chicken anti-Rat Alexa Fluor 488 (1:400, Cat#A21470, Thermo Fisher Scientific), Goat anti-Mouse Alexa Fluor 568 (1:400 Cat#A11031, Thermo Fisher Scientific), Goat anti-Mouse Alexa Fluor 488 (1:400, Cat#A21042, Chicken anti-Rat, Thermo Fisher Scientific), Chicken anti-Rat Alexa Fluor 594 (1:400, Cat#A21471, Thermo Fisher Scientific), Goat anti-Rabbit Alexa Fluor 488 (1:400, Cat#A11070, Thermo Fisher Scientific) and Goat anti-Rat Alexa Fluor 647 (1:400, Cat#A21247, Thermo Fisher Scientific). Sections were stained with Hoechst 33342 (Nacalai

Tesque) for nuclear staining and mounted using ProLong Gold Antifade Reagent (Thermo Fisher Scientific). Mounted sections were observed using a fluorescence microscope (model BZ-9000 or BZ-X710; Keyence, Osaka, Japan). The fiber cross-sectional area and number of MyHC isoform-positive fibers were determined from three animals, with a minimum of 1800 myofibers assayed per section using Hybrid Cell Count software (BZ-II Analyzer; Keyence).
All histological analysis was carried out using three independent samples.

Cell preparation and culture.

Mouse primary myoblasts were cultured according to a previously reported method (Rando and Blau, 1994; Tanihata et al., 2008). Briefly, limb muscles of 1-month-old KO ($n = 3$) male mice and littermate controls ($n = 3$) were removed and minced into a slurry in PBS using dissecting scissors. Cells were enzymatically dissociated by adding 0.2% collagenase type 2 (Worthington Biochemical, Freehold, NJ, USA) followed by passage through an 18-gauge needle and filtration through 100- and 40-μm nylon meshes (Falcon; BD Biosciences, Franklin Lakes, NJ, USA). After pre-plating for 1.5 h on non-coated dishes, primary myoblasts were cultured alone with growth medium (GM) composed of F-10 containing 20% fetal bovine serum, 1% penicillin-streptomycin (Nacalai Tesque), and 2.5 ng/ml basic fibroblast growth factor (Thermo Fisher Scientific, Waltham, MA, USA) in collagen-coated dishes (Iwaki, Tokyo, Japan). To induce differentiation, the medium was changed to differentiation medium (DM) composed of 2% horse serum in Dulbecco's Modified Eagle Medium and cultured for 4 days. GM was changed every 24 h, and DM was changed on days 1 and 3 after induction of differentiation.

Immunocytochemistry.

Differentiated primary myoblasts on day 4 after inducing differentiation were fixed with 4% paraformaldehyde in PBS and pre-incubated in PBS 3% goat serum / 1% bovine serum albumin (BSA) / 0.1% Triton X-100 for 30 min at RT. Primary antibodies in 3% goat serum and 1% BSA were applied overnight at 4°C followed by 1 hr at RT with secondary antibodies. The antibodies used were raised polyclonal for SFPQ (1:2000) (Takeuchi et al., 2018), mouse monoclonal anti-sarcomeric MyHC (1:250; MF-20, DSHB), followed by Goat anti-Rabbit Alexa Fluor 488 (1:400, Cat#A11070, Thermo Fisher Scientific) and Goat anti-Mouse Alexa Fluor 555 (1:500, Cat#A21425, Thermo Fisher Scientific). Sections were stained with Hoechst 33342 (Nacalai Tesque) for nuclear staining. Cells were observed using a fluorescence microscope (model BZ-X710; Keyence). Analysis was carried out using three independent samples.

WB (Western blotting)

Proteins were extracted from primary cells and mouse skeletal muscle tissue using sample

buffer (Nacalai Tesque), and the lysates were denatured at 95°C for 3 min, except in the case of detection of mitochondrial OXPHOS complexes. The lysates were then resolved by SDS-PAGE (SuperSep Ace gel; Wako Pure Chemical Industries) and transferred to a polyvinylidene difluoride membrane (Pall Corporation, Port Washington, NY, USA). Antibody reactions were performed with Can Get Signal immunoreaction enhancer solution (Toyobo, Osaka, Japan). Immunoreactivity was visualized with Chemi-Lumi One Super (Nacalai Tesque) or ImmunoStar LD (Wako Pure Chemical Industries) and a ChemiDoc MP imaging system (Bio-Rad, Hercules, CA, USA). The following primary antibodies were used in this study: raised polyclonal for SFPQ (1:2000 or 20000) (Takeuchi et al., 2018), mouse monoclonal antibodies cocktail for OXPHOS complexes (1:1000, Cat#ab110413, Abcam), mouse monoclonal anti-α-tubulin (1:10000, DM1A, Cat#MS-581-P1, Thermo Fisher Scientific), rabbit monoclonal anti-LaminB1 (1:1000, D4Q4Z:Cat#12586, Cell Signaling Technology, Danvers, MA, USA), mouse monoclonal anti-Puromycin (1:1000, 3RH11:Cat#PEN-MA001, Cosmo Bio Co., Ltd., Tokyo, Japan), rabbit monoclonal anti-ME3 (1:500, EPR10378:Cat#ab172972, Abcam), rabbit polyclonal anti-PHKB (1:2000, Cat#13400-1-AP, Proteintech Group, Inc., Chicago, IL, USA), rabbit polyclonal anti-GPHN (1:1000, Cat#14304, Cell Signaling Technology). Horseradish peroxidase-conjugated anti-rabbit (Cat#NA934) and anti-mouse IgG (Cat#ab5887) secondary antibodies were purchased from GE Healthcare Life Sciences (Pittsburgh, PA, USA) and Abcam, respectively.

Total RNA extraction from skeletal muscle.

GC muscles were isolated and frozen in liquid nitrogen. Frozen muscle tissues were powdered in liquid nitrogen, lysed by Buffer RLT (QIAGEN, Valencia, CA, USA), and digested by proteinase K. Total RNA was extracted using an RNeasy mini kit (QIAGEN) according to manufacturer protocol.

Reverse Transcription-quantative Polymerase Chain Reaction (RT)-qPCR.

First-strand cDNAs were synthesized with random primers (Takara, Shiga, Japan), and qPCR was performed using FastStart Universal SYBR-Green Master (Hoffmann-La Roche, Inc., Nutley, NJ, USA) according to the manufacturer's protocol. Cell culture data were normalized to *TATA box binding protein* (*Tbp*) expression. Mouse data were normalized to *hypoxanthine guanine phosphoribosyl transferase* (*Hprt*) expression. PCR primer pairs were as follows.

Dmd 3' F (HO255)	CTCTCCATTTCACAGCATACCAC
Dmd 3' R (HO256)	AAACCGTGGATAAGTGCTCTATG
Dmd 5' F (HO261)	CCCTCCATTCTAACCGATGTG
Dmd 5' R (HO262)	ATTTGATCACACAGGTATGCGC

Acyp2 3' F (H0583)	AGCCAACCCAAGATTAGCAGGC
Acyp2 3' R (H0584)	GTTCCGAGGTCAGCGTCTGTAAC
Acyp2 5' F (H0585)	ACTTTGTCAGAGGTTGTAGCCCC
Acyp2 5' R (H0586)	TGGCCTGGGAGTGTACTTCAGC
Ahcyl2 3' F (H0607)	TTGTCCTAAGTCTGTCTGCACGG
Ahcyl2 3' R (H0608)	AGTAAAGCGCCCAATGGCTCAC
Ahcyl2 5' F (H0609)	CTCGGGAAACCCTCTGAGTTGC
Ahcyl2 5' R (H0610)	TGCAATGGCTAGAAAGGAAGGGC
Esrrb 3' F (H0655)	TTCCCAGCTTAACGAACCCAGC
Esrrb 3' R (H0656)	CTGCCTTTCCAGGTACAGCTCC
Esrrb 5' F (H0657)	AAAGCATCCATCCCTGTGTGGC
Esrrb 5' R (H0658)	GGGACCCACTGATTCCAAACGAG
Esrrg 3' F (H0699)	GTTGCATCCGCACTTGGCTTG
Esrrg 3' R (H0700)	AATCACTCCCCTGCCAACAAGG
Esrrg 5' F (H0663)	TGTCTGGTGCCTTTTGTGTGGAG
Esrrg 5' R (H0664)	CCAGCGCCTATTCTTAGCACCTG
Gmds 3' F (H0625)	GATTTGGGGTGGGAGCACATTTAC
Gmds 3' R (H0626)	AAGGGAGACCCACATAGCTGGAC
Gmds 5' F (H0627)	GGCATGAACTCCTTGGGTGAGG
Gmds 5' R (H0628)	GCAGTGGTTAGCCTTATCTGTTGC
Gphn mRNA F (H0635)	ACTCCGGTGCTTGGTACAGAAATC
Gphn mRNA R (H0636)	ATCAGCAGCTCGAACAGCATAGCC
Gphn 3' F (H0631)	TGACTGAATAGGAGAAAGAAGACAC
Gphn 3' R (H0632)	ACCCATTTTCACTGAGGTTTGAGC
Gphn 5' F (H0633)	CTGCATGTCTGATTCCGTTGCG
Gphn 5' R (H0634)	GAACCTCAGCCGAAACCCCTAC
Hs6st2 3' F (H0691)	TTCATGCCTGGTGTGGATACGG
Hs6st2 3' R (H0692)	AGGTGGTGGCATCTGTTCTGTG
Hs6st2 5' F (H0693)	CCGCAAGGACTGGACACTACAC
Hs6st2 5' R (H0694)	AACAAGCCTGGTCTTTGGGACC
Maob 3' F (H0601)	CACCTTCTGGAATGACTCCCACC
Maob 3' R (H0602)	CCAGCTCTTCAAGGTTCTTTACTCC
Maob 5' F (H0603)	CAGGTCCAAAGACTGCCCATCC
Maob 5' R (H0604)	CATGGAGTCTGCCTGACCTTCC
Me3 mRNA F (H0581)	CTGTCCTGCTAGATGTTGGCACC
Me3 mRNA R (H0582)	TCATCATACTCCTCCCCACGGAC
Me3 3' F (H0673)	TCACAATGTCGGTACAAGGAGCC
Me3 3' R (H0674)	CAGCCTGGAGTATGATGGAGGAC
Me3 5' F (H0579)	GGGCTTGGGACGAAACCTATGG
Me3 5' R (H0580)	TCTCCATGTCAAGAGGGGGACG
Nmnat3 3' F (H0619)	GACTAAACCCCACAGGACTGCC

Nmnat3 3' R (H0620)	TCTCTGGACAACTAACAGGCCAC
Nmnat3 5' F (H0621)	AAGCCACTGTTCTAAGATGGGACTG
Nmnat3 5' R (H0622)	GAGATACCTTCACCCCTGCTGTG
Phkb mRNA F (H0563)	ACCAACTTTGTCGGATATGACC
Phkb mRNA R (H0564)	CCAGTTCAGGGTTTCTTTCCAGC
Phkb 3' F (H0677)	AATCTGTGGCCTTTGACCTGGC
Phkb 3' R (H0678)	TCATGCTCGCTCTTGGGAAGAC
Phkb 5' F (H0561)	GAAATTGGCCCCTTCCCTAGCC
Phkb 5' R (H0562)	GTTCAGGACACTCGGACTGCTG
Plce1 3' F (H0717)	TTACGGTGCCACAAAGTAGCGAG
Plce1 3' R (H0718)	TGGTCCCACTAGAAGCTCTTTTGG
Plce1 5' F (H0639)	TGTCTATTAGCTTTGGCGAGGC
Plce1 5' R (H0640)	AGGGAGAAGAGAGGAAAGACGGAC
Ppargc1b 3' F (H0649)	CTCAGAGTTTCCTGGGGAGCAG
Ppargc1b 3' R (H0650)	ACATGGGATGAACCTATCGCCC
Ppargc1b 5' F (H0651)	TCCTCCCGCAGGTAGAATCCAG
Ppargc1b 5' R (H0652)	AAAGTACGGCAGCAAGTGCCAG
Suclg2 3' F (H0679)	TTGGAGTGCCAGGGACAATACAG
Suclg2 3' R (H0680)	CTTTTCAGATATGCCCGGCTGAC
Suclg2 5' F (H0591)	GAGGTTTCTCAGCCGCTTACTGG
Suclg2 5' R (H0592)	ACAGACAAGCACAAGGGGGTC
Idh1 3' F (H0667)	TTTTGAAACCTACTCTTCGGGC
Idh1 3' R (H0668)	TGCACACATTCACAGGAGACCC
Idh1 5' F (H0669)	GATGAACTCAGTGGCAAGGCCC
Idh1 5' R (H0670)	CTCCCAAAGCGATCCCAACCTC
Tbp-F (H0681)	ATCAGATGTGCGTCAGGCGTTC
Tbp-R (H0682)	CGTCTTCAATGTTCTGGGTTATCTTC
Gbe1 3' F (H0565)	ACGTGCTAGTCTGAGGGGACAC
Gbe1 3' R (H0566)	AGCACAAGCCGGTGAACTCAAG
Gbe1 5' F (H0567)	TCTTGCACCCTCCTGTTTGCTC
Gbe1 5' R (H0568)	GCAAAGGTCGCTCTTCGATGTTG
Hlcs 3' F (H0595)	GTGTGCTCGTTTTCCTTTGCCC
Hlcs 3' R (H0596)	TGGGCTTCGGGTCTGCTTTTAG
Hlcs 5' F (H0597)	ACTCACCCTTTAGGAACACCGC
Hlcs 5' R (H0598)	TACTGTTGTGCTGGCTCTGACG
Pcca 3' F (H0701)	TCAGGCCGACTGCGTTTATCAG
Pcca 3' R (H0702)	CATGGCTGCACACAGACTTCTC
Pcca 5' F (H0703)	GTCCGAGCTTTACCTGCACTCC
Pcca 5' R (H0704)	GATGCCCCTTCAAAGTCGTTGC
Pcx 3' F (H0571)	GGGAGCTGTTAGCAAGAAGATGGG
Pcx 3' R (H0572)	CCACCCTTTAACCCCTGCCAAC

Pcx 5' F (HO573)	CCCACATTGGCCTTAATCCTGC
Pcx 5' R (HO574)	TGACAGACTGGAGTACGAGCCC
St3ga/3 3' F (HO643)	GAGTGCTGCTCACGACTTGATG
St3ga/3 3' R (HO644)	TTGAGGCTTTACTGGAGGCGAG
St3ga/3 5' F (HO645)	TTTGGTTAGGCGGATGTCCCAC
St3ga/3 5' R (HO646)	ACTCAGTTTTACCACCTCCCCG
Hprt mRNA F (HO199)	GGACCTCTCGAAGTGTTGGATAC
Hprt mRNA R (HO200)	GCTCATCTTAGGCTTTGTATTTGGC

RNA-seq.

Total RNA was extracted from differentiated primary myoblasts or skeletal muscles using the RNeasy Mini kit (Qiagen). The quality of isolated total RNA was examined using Agilent RNA 6000 Nano kit and BioAnalyzer (Agilent Technologies, Santa Clara, CA, USA), with RNA integrity numbers ranging from ~9.50 to 9.80 (primary myotubes) or ~7.60 to 8.70 (skeletal muscle). Total RNA (5 μg) was purified using a Dynabeads mRNA DIRECT Micro kit or a RiboMinus Eukaryote System v.2 (Life Technologies, Carlsbad, CA, USA) to prepare polyA-selected mRNA or RNA-Seq Ribo(−) RNA. Purified RNA was used for library preparation using the Ion Total RNA-Seq kit v.2 (Life Technologies). High-throughput sequencing was performed on the Ion Proton system (Thermo Fisher Scientific). Experiments were performed with biological triplicate.

Bioinformatics analysis of RNA-seq data.

We used mRNA-seq data (using polyA-selected mRNA) to evaluate gene expression. Quality controls were performed as previously described (Takeuchi et al., 2018), and reads that passed the quality control were mapped to the mouse genome sequence mm10 using STAR aligner (Dobin et al., 2013). We used the GRCm38.p4 Refseq gene model in this study. For quantification of gene expression levels, we initially calculated number of reads per 1-kb exonic genomic region per 10M reads for each gene, followed by scaling to transcripts per million (TPM) values. A gene was defined as expressed when the TPM value exceeded 2 for at least one condition. We used DEseq2 to analyze differentially expressed genes (http://www.bioconductor.org/packages/release/bioc/html/DESeq2.html.) (Love et al., 2014). Scatterplots showing average gene expression levels in *Sfpq* KO and control samples and relationships between FCs in gene expression and pre-mRNA lengths were tested and plotted using the R statistical package (http://www.r-project.org/).

Bioinformatics analysis of RNA-seq Ribo(−).

Bioinformatics analysis was performed as previously described (Takeuchi et al., 2018), with some

modifications. For visualization using the Integrated Genome Browser (http://bioviz.org/igb/), we prepared 10-kbp windows and calculated the RPK10M and relative expression values for KO vs. control myotubes for only intron reads from RNA-seq data. We determined pre-mRNA ratios between KO and control myotubes by calculating the average depths of RNA-seq reads using a window size of 10 kbp. We split mapping results (BAM files) into exon-mapped reads and others (i.e., mainly intron-mapped reads) with samtools (http://www.htslib.org/), and reads mapped to exons were excluded to detect changes in pre-mRNA levels. Relative expression values were smoothed around +4 regions.

GSEA.

Expressed genes (10,810 genes; TPM ≥ 2.0 for at least one condition) were used as input for GSEA (http://software.broadinstitute.org/gsea/index.jsp) (Subramanian et al., 2005) using GSEA 2.0 with default parameters (except for the permutation type, which was changed to "gene set") and the KEGG and Reactome gene sets from the Molecular Signatures Database curated gene sets (v.6.0; http://software.broadinstitute.org/gsea/msigdb/). The "METABOLIC_PATHWAYS" gene set from KEGG pathway mmu01100 was added to the KEGG gene sets. Gene symbols in the KEGG and Reactome gene sets were changed to mouse-specific gene symbols in mm10.

Statistics.

Values are presented as mean ± SD or SEM. Statistical significance was evaluated with a two-tailed Student's or Welch's t test to analyze differences between two experimental groups ($p < 0.05$ was considered significant). In Figure 1F, 3A and S3A, statistical significance was evaluated with Mann-Whitney U test ($p < 0.01$ was considered significant). Statistical analysis of RNA-seq was evaluated with DEseq2 to analyze differentially expressed genes (http://www.bioconductor.org/packages/release/bioc/html/DESeq2.html.) (Love et al., 2014). Statistical analysis of GSEA data was evaluated with GSEA 2.0 (http://software.broadinstitute.org/gsea/index.jsp) (Subramanian et al., 2005) with default parameters (except for the permutation type, which was changed to "gene set").

Data and Software Availability.

RNA-seq data are registered in the NCBI SRA with accession number GSE106827. For calculating reads per kilo base per million mapped reads (RPKM) and TPM in-house scripts were used. All data and scripts not included here are available from the corresponding author upon reasonable request.

Supplemental References

Bothe, G.W., Haspel, J.A., Smith, C.L., Wiener, H.H., and Burden, S.J. (2000). Selective expression of Cre recombinase in skeletal muscle fibers. Genesis *26*, 165-166.

Chan, T.M., and Exton, J.H. (1976). A rapid method for the determination of glycogen content and radioactivity in small quantities of tissue or isolated hepatocytes. Anal. Biochem. *71*, 96-105.

Dobin, A., Davis, C.A., Schlesinger, F., Drenkow, J., Zaleski, C., Jha, S., Batut, P., Chaisson, M., and Gingeras, T.R. (2013). STAR: ultrafast universal RNA-seq aligner. Bioinformatics *29*, 15-21.

Goodman, C.A., Mabrey, D.M., Frey, J.W., Miu, M.H., Schmidt, E.K., Pierre, P., and Hornberger, T.A. (2011). Novel insights into the regulation of skeletal muscle protein synthesis as revealed by a new nonradioactive in vivo technique. FASEB J. *25*, 1028-1039.

Iwasaki, H., Naka, A., Iida, K.T., Nakagawa, Y., Matsuzaka, T., Ishii, K.A., Kobayashi, K., Takahashi, A., Yatoh, S., Yahagi, N., et al. (2012). TFE3 regulates muscle metabolic gene expression, increases glycogen stores, and enhances insulin sensitivity in mice. Am. J. Physiol. Endocrinol. Metab. *302*, E896-902.

Love, M.I., Huber, W., and Anders, S. (2014). Moderated estimation of fold change and dispersion for RNA-seq data with DESeq2. Genome Biol. *15*, 550.

Malicdan, M.C., Noguchi, S., and Nishino, I. (2009). Monitoring autophagy in muscle diseases. Methods Enzymol. *453*, 379-396.

Matsuo, N., Tanda, K., Nakanishi, K., Yamasaki, N., Toyama, K., Takao, K., Takeshima, H., and Miyakawa, T. (2009). Comprehensive behavioral phenotyping of ryanodine receptor type 3 (RyR3) knockout mice: decreased social contact duration in two social interaction tests. Front. Behav. Neurosci. *3*, 3.

Miyakawa, T., Yamada, M., Duttaroy, A., and Wess, J. (2001). Hyperactivity and intact hippocampus-dependent learning in mice lacking the M1 muscarinic acetylcholine receptor. J. Neurosci. *21*, 5239-5250.

Quinlan, K.G., Seto, J.T., Turner, N., Vandebrouck, A., Floetenmeyer, M., Macarthur, D.G., Raftery, J.M., Lek, M., Yang, N., Parton, R.G., et al. (2010). Alpha-actinin-3 deficiency results in reduced glycogen phosphorylase activity and altered calcium handling in skeletal muscle. Hum. Mol. Genet. *19*, 1335-1346.

Rando, T.A., and Blau, H.M. (1994). Primary mouse myoblast purification, characterization, and transplantation for cell-mediated gene therapy. J. Cell Biol. *125*, 1275-1287.

Subramanian, A., Tamayo, P., Mootha, V.K., Mukherjee, S., Ebert, B.L., Gillette, M.A., Paulovich, A., Pomeroy, S.L., Golub, T.R., Lander, E.S., et al. (2005). Gene set enrichment analysis: a knowledge-based approach for interpreting genome-wide expression profiles. Proc. Natl. Acad. Sci. U. S. A. *102*, 15545-15550.

Takeuchi, A., Iida, K., Tsubota, T., Hosokawa, M., Denawa, M., Brown, J.B., Ninomiya, K., Ito,

M., Kimura, H., Abe, T., et al. (2018). Loss of Sfpq Causes Long-Gene Transcriptopathy in the Brain. Cell Rep. *23*, 1326-1341.
Tanihata, J., Suzuki, N., Miyagoe-Suzuki, Y., Imaizumi, K., and Takeda, S. (2008). Downstream utrophin enhancer is required for expression of utrophin in skeletal muscle. J. Gene Med. *10*, 702-713.